Citation
Rahman, S.A. and Shaikh, F.U.A. and Sarker, P.K. 2022. A comprehensive review of properties of concrete containing lithium refinery residue as partial replacement of cement. Construction and Building Materials. 328: ARTN 127053. http://doi.org/10.1016/j.conbuildmat.2022.127053

A comprehensive review of properties of concrete containing Lithium refinery residue as partial replacement of cement

Sm Arifur Rahman, Faiz Uddin Ahmed Shaikh* and Prabir Kumar Sarker

School of Civil and Mechanical Engineering, Curtin University, Perth, Australia

*Corresponding author Email: s.ahmed@curtin.edu.au

Abstract

The escalating demand for lithium battery products in making electronic devices is producing an enormous amount of lithium refinery residue (LRR). This waste is not only an environmental hazard, but most importantly, its proper disposal is very costly. The high cost of Li-battery can be reduced by utilizing this waste in concrete to produce new smart materials in an engineered way to obtain a greater life cycle. The study aims at unravelling a new generation of material that enables its optimization in concrete. Specifically, this paper presents a comprehensive review of physio-chemical properties of some common supplementary cementitious materials (SCMs) and their comparisons with LRR. The previous studies recommended to use 10-20% LRR as a SCM which is suitable for concrete by capturing complex properties like fresh, mechanical, durability and microstructural in line with other pozzolanic materials.

Keywords: Lithium refinery residue; Pozzolanic material; Silica-rich wastes; Sustainable recycling.

1. Introduction

Lithium batteries are ubiquitous and have gained unyielding reliability in making clean energy source for smart devices and vehicles [1]. Though different types of batteries are available in the market, unsurprisingly, the insatiable industrial demand for the

lithium compound is still immutable. At present, pristine lithium compounds are extracted mostly from spodumene ore and to some extent from lepidolite. Spodumene is indigenous in a very limited deposit in Chile, Australia, China, Argentina, Brazil, USA, Zimbabwe, and Portugal. After Chile, Australia possesses the second-largest lithium reserve, and Western Australia (WA) supplies the highest lithium in the global battery market [2]. Lithium refinery residue (LRR), and various metal oxides are generated as by-products after the chemical treatment of spodumene to produce lithium carbonate. The current lithium production process generates about 9-10 tons of LRR in the production of one ton of lithium carbonate [3-6]. Australia produced 42,000 tons of lithium in 2019, and the produced LRR covered a large area of backfill [2, 7]. This hazardous waste is not only an environmental threat but most importantly, its proper disposal is very costly. The high cost of Li-ion battery can be reduced by using LRR as a supplementary cementitious material (SCM) in concrete to produce new low-carbon concrete in an engineered way.

The mineralogical composition of LRR shows high amounts of the oxides of silicon, aluminum, and calcium which directed the material scientists to use LRR as a partial replacement for Ordinary Portland Cement (OPC). The reduction of cement as a binding material in concrete production reduces the carbon footprint, health hazard, and construction cost. The use of LRR as SCM will start a new circular economy.

Different terminologies are used by different researchers to represent the material lithium slag/ delithiated spodumene/ delithiated β spodumene and the term LRR is used in this paper. Several research articles are available in literature on the use of LRR as a new SCM. It has been found that a substantial amount of work has been

conducted in China on the use of this material in concrete. Previous studies considered binary, ternary, and quaternary combinations, such as LRR-cement [5, 8-16], LRR-fly ash (FA) [16-19], LRR-silica fume (SF) [4], LRR-triisopropanolamine (TIPA) [20], LRR-limestone powder (LP) [21, 22], LRR-crushed limestone [11, 23], LRR-iron slag [19], LRR-ground granulated blast furnace slag (GGBFS) [17], and LRR-GGBFS-FA [17]. The researchers used LRR as a SCM in both dry [3-5] and wet [10, 14, 24] state of mixing. The investigators studied the properties of concrete [9, 11, 16] while minuscule works on pastes [18, 25] and mortars [14, 20, 24] that will lead to a future research arena. Besides, the use of LRR was also attempted in alkali-activated geopolymers [26-31], backfill [18, 25] and brick [32].

Researcher covered a wide range of physio-chemical tests of LRR. The investigations include visual classification [33], specific surface area [5, 8, 15], specific gravity [4, 5], density [28], moisture content [15, 16], particle size distribution [13, 14, 24], chemical composition [3-5], X-ray diffraction (XRD) [13, 14, 20], scanning electron microscopy (SEM) [14, 24, 26], Fourier-transform infrared spectroscopy (FT-IR) [13], inductive couple plasma (ICP) [33], nuclear magnetic resonance (NMR) [14, 33], X-ray photoelectron spectroscopy (XPS) [14], and thermogravimetry (TGA) [3, 28].

The fresh properties included setting times [10, 20], fluidity [4, 12], workability [18, 20], , air content [15, 16], density [15-17], bleeding [15, 16], and electrical conductivity [10] and hydration heat [14, 20, 24]. Again, the mechanical properties included compressive strength [3-5], tensile strength [19, 34, 35], elastic modulus [5, 34], and flexure strength[3, 8]. The durability properties consist of alkali-silica reaction (ASR) [16], chloride migration [9, 12, 19], sulfate attack [3], shrinkage [5, 12], water loss [14,

23], pH [26], and creep [5]. In addition, the microstructural properties comprised of Scanning Electron Microscopy (SEM) [3-5], Energy Dispersive X-ray Spectra (EDS) [3, 13], X-ray Powder Diffraction (XRD) [3-5], nanoindentation [4, 36], Thermogravimetric Analysis (TGA) [3, 14], Differential Scanning Calorimetry (DSC) [12, 13], Fourier-transform infrared spectroscopy (FT-IR) [27-29], Nuclear Magnetic Resonance (NMR) [28, 29], N_2-adsorption [28], and Mercury Intrusion Porosimetry (MIP) [5, 11].

This study presents an analysis of the physio-chemical, mechanical, durability, and microstructural properties of the products of LRR. Recommendations are made on the sustainable use of the LRR in concrete with identification of the needs of future works.

2. Physiochemical and microstructural properties of raw LRR

The physical properties of a SCM influence the fresh, mechanical, durability and microstructural properties of concrete. Researchers covered the in-depth physical properties to meet the sustainable challenges. Thus, in this study, the physical properties of some other common SCMs, such as Kaolin (KA), Metakaolin (MK), GGBFS, Ferro-nickel slag (FNS), Cement and FA were considered along with LRR to understand various considerations that are required to implement a SCM as a sustainable product. The physiochemical and microstructural properties comprised particle size, fineness, chemical composition, XRD, SEM, and TGA.

2.1 Particle size distribution, fineness, and chemical compositions

The particle size distribution (PSD) of LRR varied depending on the source. The PSD is categorized into 10% (d10), 50% (d50) and 90% (d90) finer than the size in order to

compare the grain distribution of LRR with other common SCMs. The variation of the particle size of the SCMs is illustrated in Fig. 1 from different literatures [24, 26, 37-39]. LRR was found as the coarsest among all SCMs, while MK was the finest in the same comparison. The d10 of LRR was 4.47 μm while that of MK was 0.94 μm. The median particle size of FA, GGBFS, and FNS was roughly closer to that of cement (16.25 μm). All the SCMs under consideration were well-graded, as defined by the coefficient of uniformity (C_u = d60/d10) such that KA (C_u >3.62) and FNS (C_u >13.31). The C_u of LRR was greater than 9.03. The d90 of LRR and FNS were approximately 2.5 and 2 times the cement particle size.

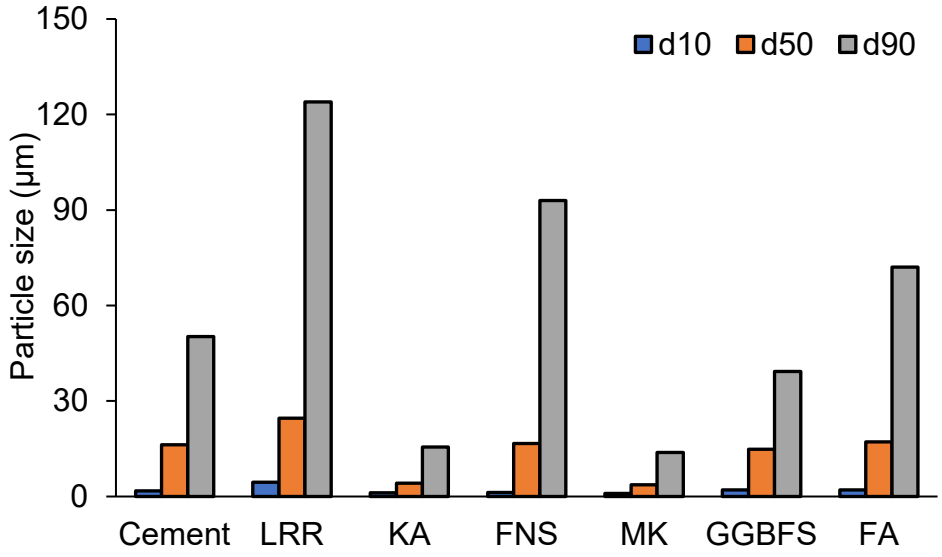

Fig. 1: Particle size of different cement and SCMs (Source: Cement [37], LRR [24], KA [26], FNS [38], MK [39], GGBFS [26], and FA [39])

From previous research, it is seen that D10 of LRR varies from 0.13 to 20 μm and the median was 1.77 μm. Similarly, the D50 had a range of 0.3 to 171 μm, and the median of D50 was 10.7 μm. Besides, D90 was reported 0.66-180 μm and the median size was escalated to 54.5 μm. Some researchers conducted dry [8] and wet grinding [10,

14, 24] of LRR to decrease the grain size and increase amorphousness. Wet grinding of 60 and 120 minutes gave higher ion dissolution than the raw sample and enhanced higher amorphousness of the bulk sample [10, 14]. Consequently, the reactivity of the LRR increased, and a small percentage of wet grinded pozzolanic material as a SCM could perform better than the higher percentage of raw sample. A 120-minute wet grinding increased the molar concentration of aluminum, silicon, and lithium by 645, 134, and 37 times compared to the raw LRR. The binding energy of the elements was analyzed in X-ray photoelectron spectroscopy (XPS) [14]. The 120 minutes wet grinding reduced the binding energy of aluminum and calcium, while the silicon was increased. This enhanced the expedited formation of ettringite (AFt), secondary ettringite (AFm), C-S-H, and N(C)-A-S-H gels. On the other hand, the fineness of the LRR by different researchers varied from 400 to 1800 m^2/kg, and the median value was 473 m^2/kg. The density was 2450-2500 kg/m^3, and the median value was 2490 kg/m^3. The loss on ignition of LRR at 750^oC was found to vary from 0 to 33% with a median value of 7.65%.

The chemical composition of a SCM is an important parameter to assess the performances of paste, mortar, and concrete. The chemical compositions of SCMs can be determined by X-Ray Fluorescence (XRF) and Quantitative XRD (QXRD) tests. Fig. 2 presents the normalized ternary representation of the summation of oxides in different axes. The horizontal axis represents the sum of silicon, aluminum, and ferric oxides. As per ASTM C618 [40], the sum of these three oxides must be greater than 70% for a pozzolanic material. The other axes are calcium oxide and the sum of magnesium, sodium, potassium, and sulfur oxides, respectively. The calcium oxide is

separated as an axis to represent the lime content that may enhance the binding capacity of the SCM.

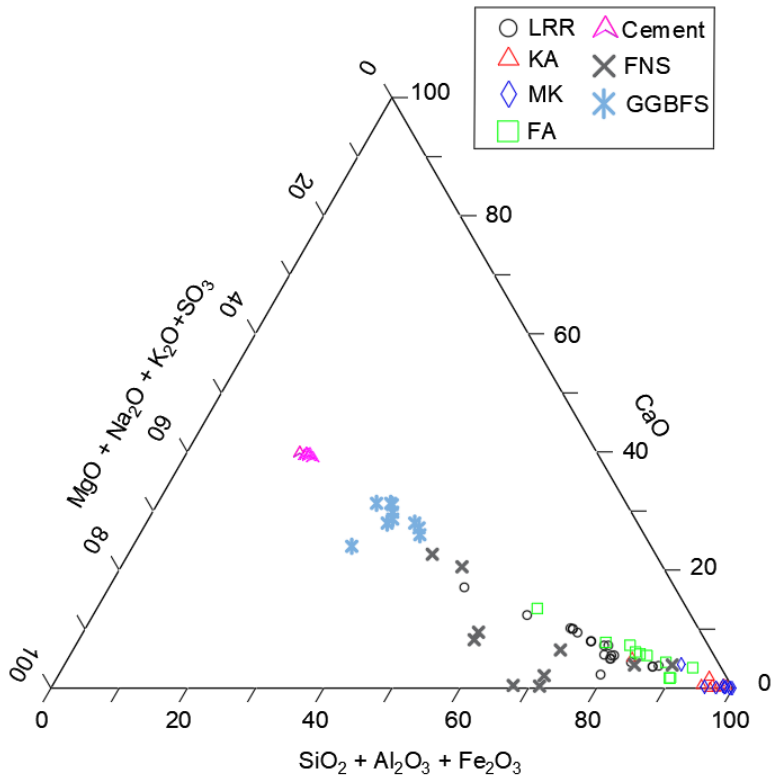

Fig. 2: Ternary graph of summation of oxides for different pozzolanic materials used by different researchers (combined and reproduced).

The chemical compositions of LRR are compared with the KA [41-50], MK [51-60], FA, FNS [61-68], FA [69-75], and GGBFS [76-84]. It is evident from Fig. 2 that the increasing order of calcium oxide by SCMs are MK, FA, KA, LRR, FNS, and BFS. The normalized value of LRR calcium oxide is approximately 0.15-0.50, which is greater than MK, FA, and KA. The pozzolanic activity of the SCMs is in the opposite order of the calcium oxide content as observed from the horizontal axis of the ternary graph. LRR pozzolanic activity oxides' normalized value is from 0.52 to 0.85, and the value is greater than those of FNS and GGBFS. The sum of other oxides for all SCMs are ranging approximately from 0.01 to 0.45, and the LRR has the value of approximately

from 0.09 to 0.31. In Fig. 2, all SCMs under considerations are literally categorized according to calcium oxide content. The highest lime content is in GGBFS, and the lowest content is in ferro-nickel slag (FNS), kaolin, and metakaolin, while LRR had a moderate lime content.

2.2 Microstructural analysis of LRR

The XRD of LRR showed gypsum, quartz, sodium aluminosilicate, and complex oxide of calcium, aluminum, silicon, sodium, and potassium. Yiren et al. [33] indicated that LRR contained an amorphous aluminosilicate phase from 39.78-42.65%, crystalline phase from 34.41-44.74%, and gypsum from 6.46-9.83% by analyzing the BSE image (Fig. 3).

Fig. 4 shows the microscopic images of different SCMs under consideration. The images are derived from different literatures and referred to in the image description with their respective scaling. From the SEMs, it is observed that only FA microscopic particles are spherical and others are irregular. The kaolin is calcined at 700-900^{o}C to produce MK and after that micro-particle image was taken. The SEM images of KA, and MK are similar, and there is a similarity of the particle shapes in GGBFS and LRR. The SEM of LRR is shown in Fig. 4 (a). LRR composed of irregular particles, and the long rod-like shape indicates the gypsum. The particle shape of GGBFS is also irregular. On the other hand, grains of MK were stacked like cotton fiber. The SEM of FNS is illustrated in Fig. 4 (d). The microscopic image showed that a smaller number of irregular and high percentage of smaller size particles were combined uniformly. The SEM of KA is displayed in Fig. 4 (f), and the particle size is disk-like and stacked closely like cards.

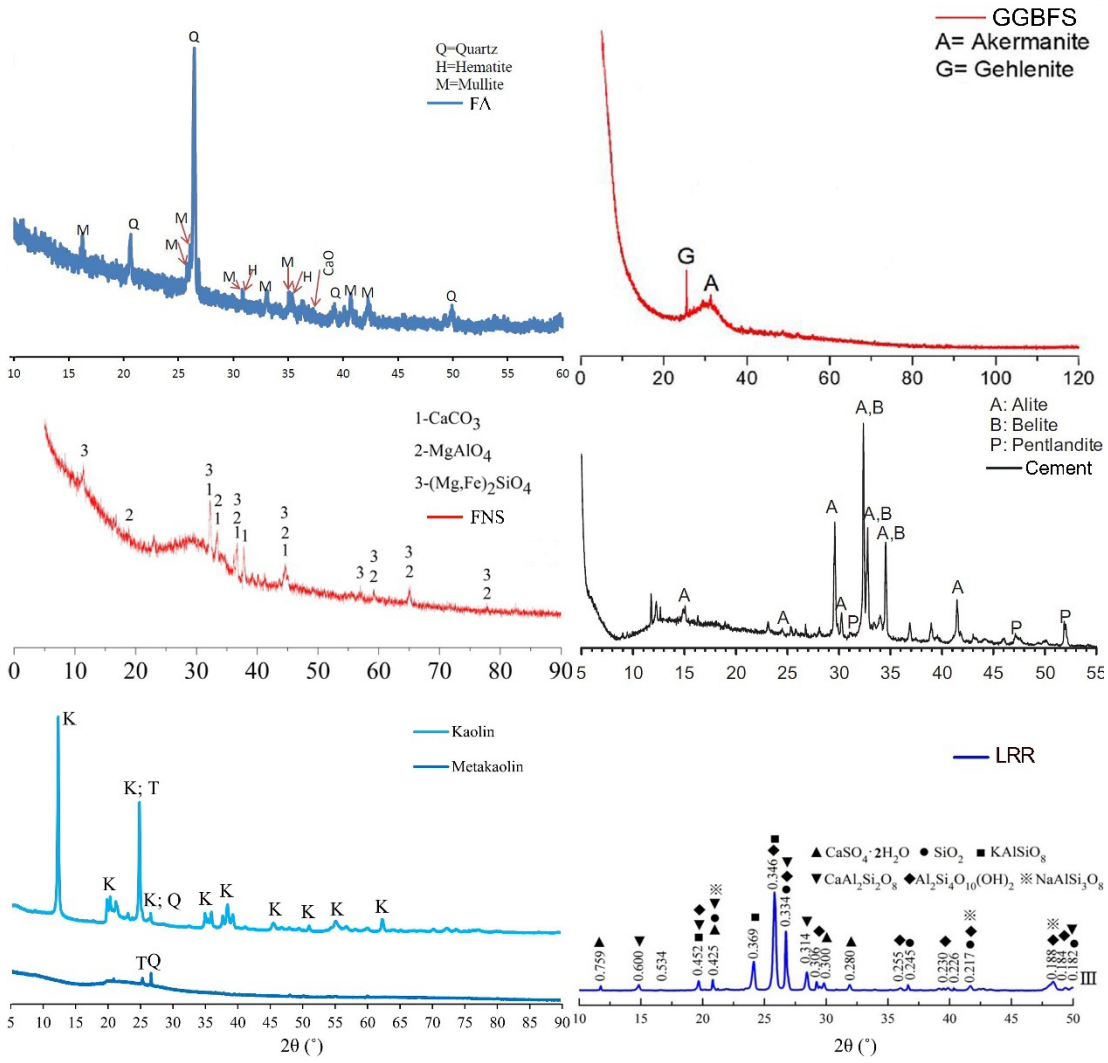

Fig. 3: Mineral composition of cement [85] and different SCMs: KA [26], MK [26], FNS [68], FA [86], LRR [33], GGBFS [87]. (Combined only)

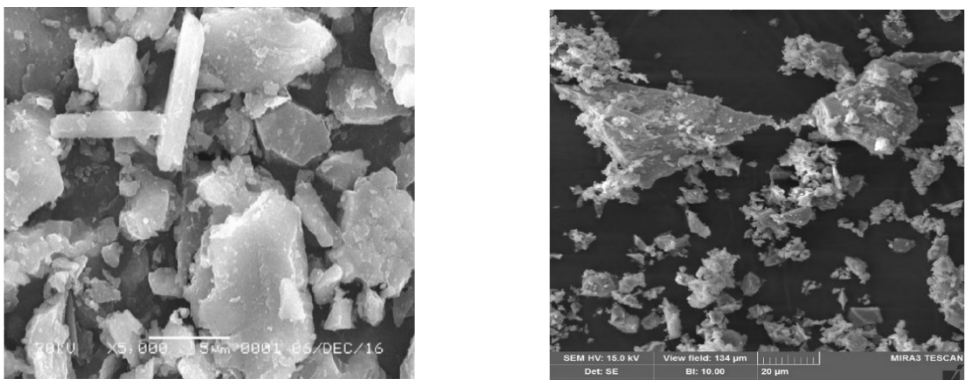

(a) (b)

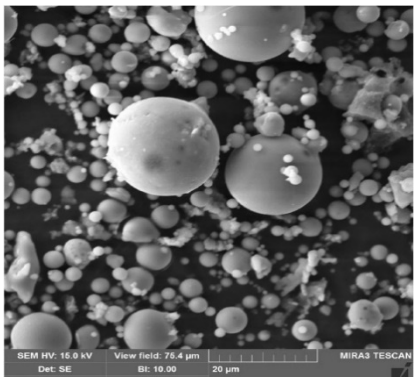

(c)

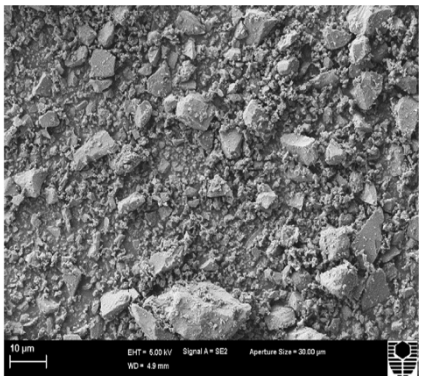

(d)

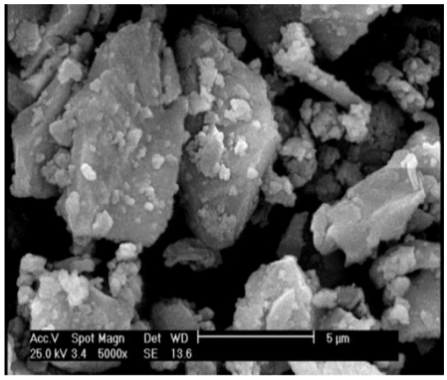

(e)

(f)

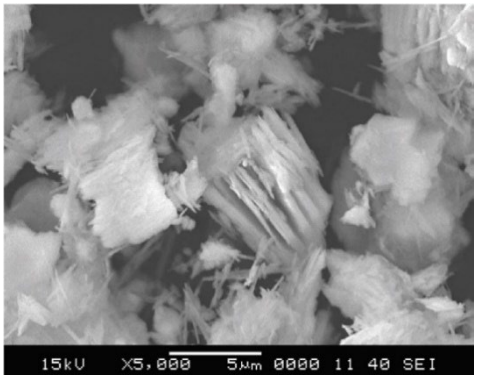

(g)

Fig. 4: SEM image of (a) LRR [5], (b) Cement [88], (c) FA [88], (d) FNS [89], (e) GGBFS [90], (f) KA [91], and (g) MK [92].

The TGA of the SCMs under consideration are plotted in Fig. 5. The TGA of different SCMs also indicated the loss of ignition indirectly. The standard specification of TGA of cementitious materials is stated in ASTM C1872 [93]. FNS had the highest mass

loss percentage, while metakaolin had the minimum. Karrech et al. [26] studied the TGA of GGBFS and indicated that the total mass loss was approximately 2.76%. A sharp reduction of mass occurred at 140°C. An approximately constant rate of mass loss is due to the decomposition of $CaCO_3$ that occurred till 1000°C. The mass loss of FA was approximately equal to GGBFS due to the burning of residual coal. Both FA and GGBFS had high thermal persistence above 800°C. On the contrary, LRR and KA had a different thermogravimetric behavior than GGBFS and FA. Both SCMs are thermally stable till 450°C and later 450-1000°C, and the mass loss of KA was higher than the LRR with respect to temperature.

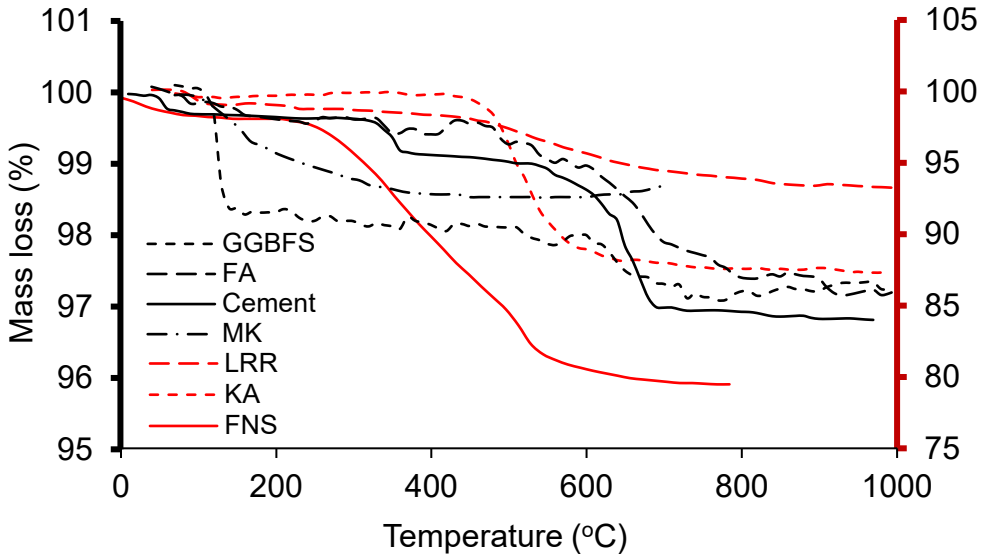

Fig. 5: TGA plot of some common SCMs: LRR [26], KA [26], GGBFS [26], FA [26], Cement [93], FNS [94], and MK [95] (combined only)

The TGA of OPC showed an erratic behavior from 400-1000°C. The decomposition of $CaCO_3$ occurred between, 400-600°C and insignificant mass loss was observed in later stages. Besides, the TGA of FNS showed an anomalous decrease of mass from 220 to 550°C. Lastly, the TGA performance of MK showed the minimum mass loss as it was previously thermally stabilized at 700-900°C from KA.

3. Fresh and hardened properties

3.1 Initial and final setting

Haigh et al. [15] designed two different strength concretes viz. 25 and 40 MPa with 25% LRR as a SCM and distinguished the setting times. The initial and final setting times of 25 MPa designed concrete were 580 and 690 minutes, respectively, while the 25% FA concrete in the same concrete design, the initial and final setting times were 280 and 420 minutes. The 40 MPa designed concrete by 25% LRR produced the same setting times and 78 and 64% higher than the control specimens. The setting time was same, and it may be due to the change of the superplasticizer content. Later, Tan et al. [10] used sulfoaluminate cement (SAC), disregarding OPC, and the setting times were dramatically reduced. Also, with the increase in LRR contents, the setting time is decreased. The findings of the study also supported by Tan et al. [24]. For 10% LRR as a SCM the setting times were 8 and 10.5 minutes, while the control specimens had 8.7 and 11.35 minutes, in the same comparison. The authors explained two possible reasons for the dramatic reduction of setting times. Firstly, SAC contains higher corundum (36.46%) than the ordinary Portland cement (4.87%) [3, 10]. The dissolved lithium salt in the LRR expediates the formation of AFt due to the use of SAC and the induction period is often disappeared [96]. Secondly, the reduction of the particle size acted as a nucleation site to induce the formation of AFt and hydration process. Munn et al. [16] studied the setting times of calcined and non-calcined LRR concrete samples compared with FA concretes. The setting times of 25% calcined LRR were 355 and 450 minutes, and the values were slightly lower than the FA and non-calcined LRR rich concretes. Tan et al. [24] used 0.5-4% nano-LRR as a SCM in cement paste specimens. The study showed that with the increase of nano LRR concentration, the

setting times were decreased rapidly. The settings times of 4% nano-LRR cement paste were 16.34 and 21.93 minutes which were approximately 33 and 37% smaller than the control specimen, respectively.

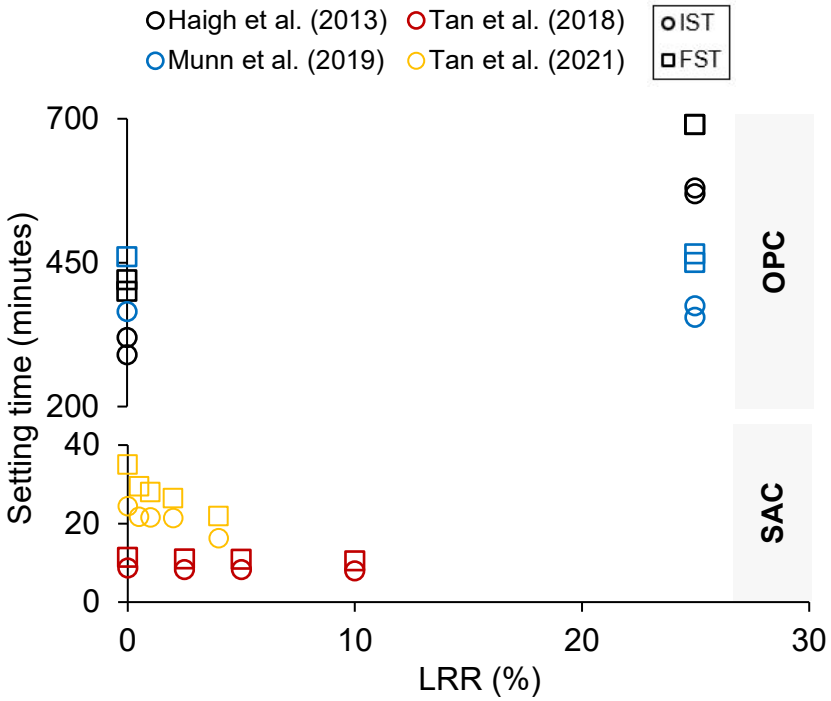

Fig. 6: Initial setting time (IST) and final setting time (FST) with respect to different lithium slag percentages by different researchers (combined and reproduced)

Fig. 6 illustrates the variation of setting times with respect to the LRR percentages. The setting times below 20 minutes are governed by the binary combination of SAC and nano-LRR in paste and mortar specimens. Lastly, the concrete samples had higher setting times (290 to 690 minutes) in comparison to the paste and mortar. Variation of the setting times was also dominant with the percentage of LRR content in the cementitious system.

3.2 Hydration

Hydration is an essential factor concerning the setting times, pozzolanic activity, and development of the strength of concrete. The isothermal calorimeter is used in the determination of hydration heat and rate. The standard practice for measuring hydration for a cementitious mixture is detailed in ASTM C1679 [97] and BS EN 196-11 [98]. Apart from isothermal calorimetry, a few researchers explained the hydration capability of LRR by using differential scanning calorimetry (DSC) [12, 13]. Tan et al. [8] used 10 minutes of grinding of 20% and 50% LRR in the determination of hydration heat rate (HHR) and total heat generation, and compared with 50% LRR (without grinding). It is seen that dry grinding increased the HHR. Again, 10 minutes dry grinded 20% LRR specimen had higher HHR till 12 hours than 50% LRR in the same comparison. 20% LRR dry grinded for 10 minutes becomes more lenient and becomes smaller than raw and 10 minutes grinded 50% LRR. Later, 0.4% sodium silicate (SS) and aluminum silicate (AS) hydrate were added separately with 20% LRR (dry grinded for 10 minutes) and compared with HHR results. Chemical conditioning initially increased the HHR but, the exothermic rate dramatically decreased after elapsing 12-hours. Tan et al. [10] compared the hydration rate of 2.5 and 10% LRR contained cement paste. The study used SAC to reduce the setting times. In addition, raw LRR was wet-grinded for 30-minutes to reduce the median particle size to 30.38 μm. The HHR of 10% LRR contained paste sample was approximately 67 and 59% higher than the control and 2.5% LRR specimens at 3 hours, respectively. While after elapsing 6-hour, the HHR of 10% LRR was dramatically reduced in the same comparison. The HHR peak shifts left when finer particles are used, and setting time is controlled by special considerations.

Tan et al. [14] examined the HHR of LRR by 120 minutes of wet grinding, which reduced the d_{50} from 24.6 to 0.30 μm. The study compared HHR of 1, 2, and 4% micro-LRR contained samples with the control. The increasing percentage of micro-LRR increased the HHR, and the elapsed time was reduced for the peak. The research finding was similar to Tan et al. [10] in terms of peak shifting. From Fig. 7 it is seen that hydration heat rates of WGLRR and nano-LRR are much higher than the rest of the samples. Sulfoaluminate cement (SAC) was used to examine the hydration heat rate of WGLRR and nano-LRR, whereas ordinary Portland cement was used in rest of the samples. It was found that addition of SAC accelerates hydration exothermic rate and advanced the appearing time of the peak by reducing the induction period significantly. The hydration heat rate of SAC dramatically accelerated by the addition of lithium salt, and the induction period almost vanishes [99]. Lithium salt develops early aluminum-lithium salt in SAC hydration; thereby accelerating the formation of AFt [99-101]. Thus, lithium ions in LRR dissolute into liquid phase where LRR plays an effective role on accelerating the early hydration of SAC.

Wang et al. [29] studied the exothermic heat generation of 3, 5, and 8% sodium-tetra-borate activated LRR samples. The study findings were deviated from Liu et al. [27], and the hydration heat consistently decreased with the addition of sodium-tetra-borate volume. Zhang et al. [20] also examined the hydration heat of 0.06 and 0.10% TIPA added with 30% LRR as a SCM. HHR of TIPA samples had two sharp picks at approximately 12 and 44 hours of the test. Interestingly, the 12 hours peak was produced by 0.10% TIPA specimen, and the latter formed by 0.06% TIPA. Tan et al. [24] compared the HHR of 2 and 4% nano-LRR with the control specimen. The study's findings were similar to Tan et al. [14] and Tan et al. [10] regarding shifting of HHR

peak. Lastly, Zhai et al. [102] studied the hydration properties of 10, 30, and 50% LRR as a pozzolanic material and compared it with the control. The study had a similar finding with Tan et al. [8] study such that HHR reduces with LRR. The study considered K-D hydration model [103, 104] for the experimental validation of the specimens.

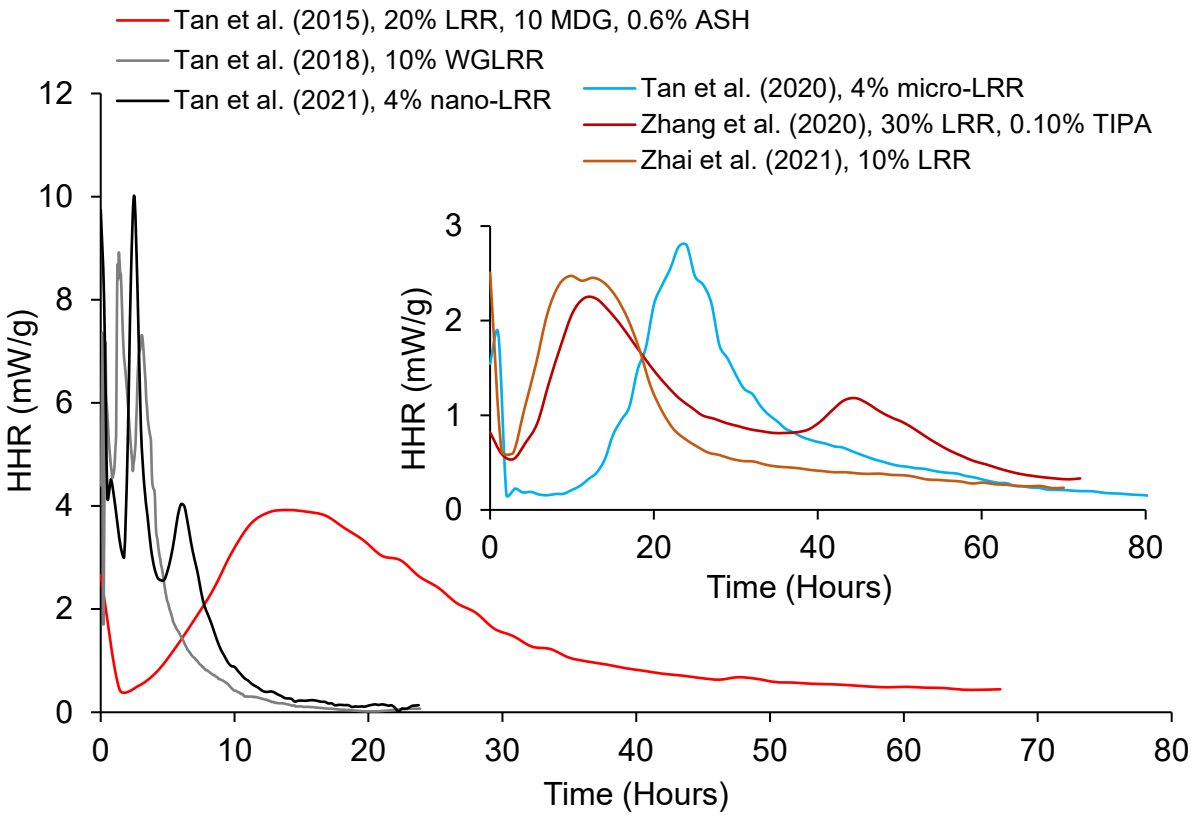

Fig. 7: Comparison of maximum LRR hydration heat rate (HHR) of various studies with respect to elapsed time (combined only)

Fig. 7 shows the exothermic heat rate of diversely processed LRR with respect to elapsed time. The figure is split into two parts to reduce the congestion of HHR data in the same plot. The SAC and nano-LRR had the maximum value of HHR while LRR conditioned with TIPA, and 120 minutes grinding were minimum among the plots. It is also noticeable that the peaks of HHR obtained are within 20 hours domain, and after that, the curve fattened down. The HHR of most of the specimens had one peak but,

there may have more than one peak. Such a system probably indicates the activation of pozzolanic material to produce much AFt and C-S-H in the system. It was highly noticeable that 30 minutes wet grinded LRR (WGLRR) had higher HHR than 120 minutes because of using SAC, the setting times of the system is reduced and thereby abruptly increased the HHR.

3.3 Fresh density, slump, mortar flow, air content, and bleeding

Huang et al. [105] studied the fresh density of LRR aero mortar with FA as a ternary combination. The study concluded that the fresh density of LRR aero mortar is low in a combination of FA. The maximum density of LRR aero mortar was 918 kg/m^3 for 100% LRR, and the density is approximately 4% higher than the 100% FA mix. Zhang and Wang [17] studied the ternary and quaternary combinations of LRR with GGBFS and FA to prepare the concrete. The binary combination of 80% GGBFS + 20% LRR had the maximum density 2532 kg/m^3 while 40% GGBFS + 40% FA + 20% LRR yielded 2493 kg/m^3. Haigh et al. [15] investigated the density of LRR concrete for 25 and 40 MPa mix designs and compared with FA and control specimens. 25% LRR as partial replacement of cement slightly reduced the concrete density in both mixes with respect to control and FA specimens.

Fig. 8 shows the variation of the slump with respect to LRR percentages from different works of literature. Shi and Zhang [35] reported that at constant water-cement ratio and superplasticizer content, the slump increased till 20% LRR content. The study reported that the slump was 186 and 196 mm for control mix and 20% LRR content specimen. When the LRR content exceeded 20% a sharp decrease of slump occurred. Haigh et al. [15] designed 25 and 40 MPa concrete mixes with water-cement ratios

0.65 and 0.5, respectively, and the slump value remained unchanged. Variable quantities of high range water reducing admixtures were used in different mix designs to keep a constant slump. Wen [22] investigated the workability of 10% LRR concrete with 10-40% lime power combinations. The increased amount of lime powder in the mix also decreased the workability. Fu-fei et al. [19] investigated concrete slump for 0.27-0.35 water-cement ratios and a ternary combination of 25-65% OPC + 15-35% LRR + 20-40% steel slag content. Slump values were not following a trend for LRR contents or water-cement ratios. When the water-cement ratio increased from 0.27 to 0.30, the slump also increased. However, at a water-cement ratio of 0.35, the concrete slump reduced. This may be due to the reduced amount of cement in the mix proportion. The relation was inversely proportional at lower water-cement ratios and higher water reducing agent content.

Later, Fu-fei et al. [106] studied the properties of HPC and showed that the slump decreased with the increase of LRR content. The study findings were not like previous studies [17, 22, 35]. The slump reduced approximately 6% for 30% LRR content at a 0.30 water-cement ratio. He et al. [23] reported a gross average 150-180 mm slump for 10-30% LRR content as a pozzolanic material. Later, Munn et al. [23] compared 25% LRR (calcined and non-calcined) and FA content concrete. The study had similar findings with Fu-fei et al. [106] and showed that 25% calcined and non-calcined LRR reduced the slump by 4 and 12%, respectively, compared with 25% FA concrete. Lastly, He et al. [11] studied 40-60% LRR content concrete and reported that the slump value remained between 180-200 mm. He et al. [11, 23] studies concluded that the workability reduces with the increase of LRR content in the mix. He et al. [4] studied the flow of UHPC with a combination of 5-15% LRR and 5-20% SF content. The flow

value was 180-200 mm for all combinations. Later, Li and Huang [12] considered the minimum mortar flow method to find the maximum LRR content used for the cement replacement. The study used 2-11% LRR as a SCM, and the flow varied from 172-225 mm. As the LRR content increased the water demand in the slurry also increases. Thus, mortar fluidity decreased, and the authors recommended to use a maximum of 11% LRR as a SCM in the mortar mix.

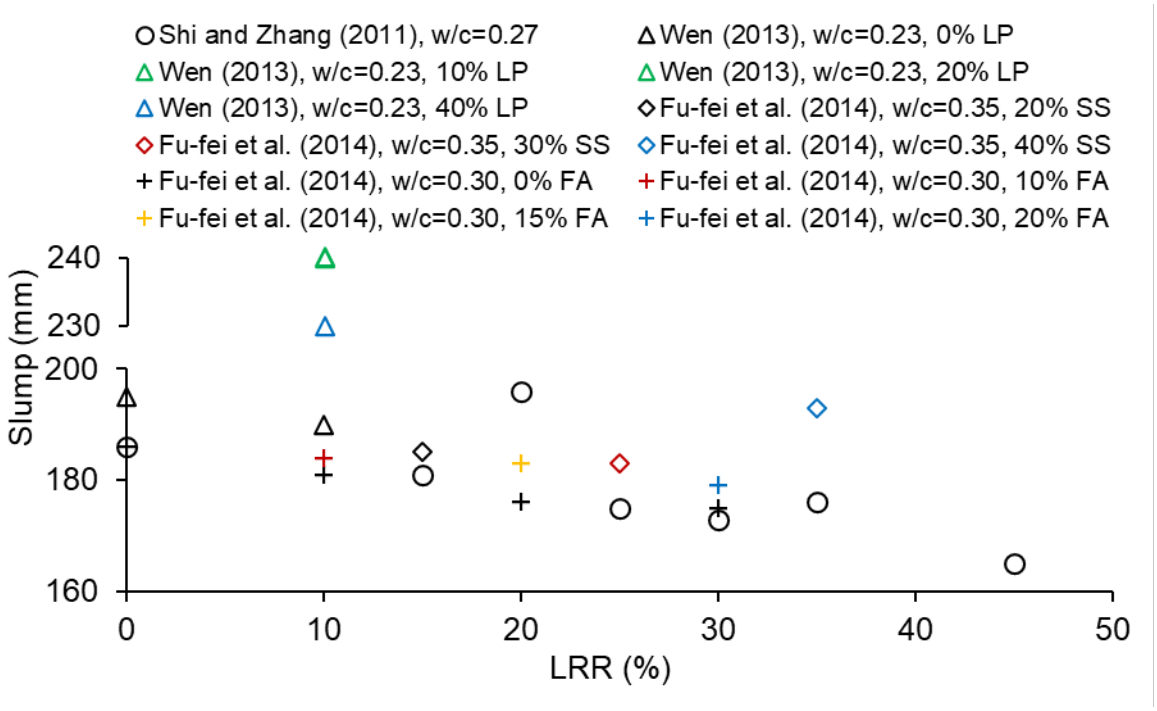

Fig. 8: Slump versus LRR content in different literatures (combined and reproduced)

Haigh et al. [14] determined the air content of 25 and 40 MPa designed LRR concretes and compared it with FA and control specimens. Both mix designs contained 25% LRR. The air content of 25 and 40 MPa LRR concretes were 2.4 and 2%, respectively. The LRR concrete air content was higher than the FA samples. The air content of control specimens was 2.0% for both 25 and 40 MPa concrete mixes. Munn et al. [22] showed that the air content of both calcined and non-calcined LRR reduced by 14%

compared to FA concrete. The findings of Haigh et al. [14] and Munn et al. [22] were directly opposite to one another. This was due to the water-cement ratio. Higher water-cement ratio increases free water in the system and more air bubbles are available for the generation. The water-cement ratio of Munn et al. and High et al. were 0.44 and 0.65, respectively. On the other hand, Haigh et al. [14] and Munn et al. [22] reported that concrete bleeding was highly reduced with the incorporation of 25% LRR as a partial replacement of cement compared to FA and control specimens.

The electrical conductivity of mortar specimens was followed by previous studies [107, 108]. Tan et al. [10] studied the electrical conductivity of wet grinded 2.5-10% wet grinded LRR mortar specimens and reported that conductivity reduced with the increase of the LRR content. The maximum conductivity of 10% LRR was 636 μS/cm at 3.5 hours, and the reading was approximately 56% lower than the control specimen. Tan et al. [14] compared the electrical conductivity of 4% micro-LRR with the control specimen. The maximum conductivity of the 4% micro-LRR conductivity was 5783.3 μS/cm at 4.5 hours, while the value of the control specimen was 6799.5 μS/cm at 4 hours. Both studies had similar findings in terms of the reduction of conductivity, which signifies dissolved ion concentration in the solution is decreased. The dissolved ion combined to form hydration products like AFt and C-S-H gel. Tan et al. [10] studied the variation of resistivity of 2.5-10% wet grinded LRR mortar for 24 hours and reported the proportional relationship of resistivity and conductivity. Initially, the growth of resistivity of the control specimen was slower than the LRR containing specimens, and after an elapsed time of 8 hours, the resistivity of all LRR specimens became flat with respect to time. The mortar containing 10% LRR had the lowest resistivity (48 Ω.m), and the value was approximately 28% less than that of the control specimen.

4. Mechanical properties

4.1 Compressive strength

Li et al. [21] studied the 10, 20, and 40% cement replacement by LRR with 10% lime powder to produce concrete. For a 10% substitution, the maximum strength activity index (SAI) was 121% at 28 days, and the maximum compressive strength was 139 MPa at 180 days. Haigh et al. [15] used 25% LRR as a SCM for 25 and 40 MPa concrete mixes. The results indicated that pozzolanic activity of LRR remained dormant till 28 days. The SAIs of LRR concrete were 113% and 99% for two different concrete mixes on 28 days test, respectively. Wen [22] studied a ternary combination with limestone powder (10-40%) and LRR (10%). The 28- and 60-days compressive strengths of ternary specimens decreased by 24-54% and 2.5-29%, respectively, compared to the control specimens. Surprisingly, 3- and 7-days SAI of 10% limestone + 10% LRR as SCM were 131% and 118% compared to 10% LRR as a cement replacement.

Later, Wu et al. [19] used 10-20% fly ash and 10-30% LRR combinations as partial replacement of cement in concrete specimens. For 10% fly ash +10% LRR, the SAI was slightly higher (1.0-3.6%) than 10% LRR on 3, 7, 28 and 90 days, respectively. The SAI for 20% fly ash + 30% LRR were approximately 100% in both 28- and 90-days test in comparison to the control specimen. Tan et al. [8] found that the early age and long term compressive strength depended on dry grinding time and the percentages of LRR as a SCM. It is seen that dry grinding time had negative effects on both early age and 28 days strength developments. The 28 days SAI for 50% LRR with 10 minutes grinding gives 85% compared to the ungrounded sample. The study

also used two different accelerators, viz. sodium and aluminum silicate with 20% LRR as a SCM and considered 10 minutes grinded samples with a varying concentration of 0.4-0.8%. For all concentrations, aluminum silicate induced a slightly higher compressive strength than sodium silicate. He et al. [5] used 10-30% LRR in making concrete specimens as a partial replacement of cement to investigate long-term compressive strength. The research indicated that for a 20% cement replacement by LRR, the compressive strength increased by 7.12% and 9.57% on 60- and 90-days compressive strength, respectively, compared to the control specimen. He et al. [4] studied the addition of LS and silica fume in the ultra-high strength concrete (UHSC) as a ternary combination without coarse aggregate. The mix combinations were 0% LS + 20% SF (control specimen), 5% LS + 15% SF, 10% LS + 10% SF, and 15% LS + 5% SF, respectively and 40 mm cubes were used for the determination of mechanical properties. The study found that the 10% LS + 10% SF mix exhibited the highest compressive strength at 28 and 90 days compared to the control specimen by 4% and 7%, respectively.

Research showed that 30- and 120-minutes wet grinding increased ion dissolution of silicon, aluminum, and lithium concentrations from 21.84-134.4, 132.3-644.5, and 5.97-36.5 times, respectively [4, 14, 24]. Increased concentration of elements also induces material amorphousness and pozzolanic activity. This enhances mortars' early- and long-term strengths with a lower volume of LRR (0.5-10%) in cement mortar compared to past studies. For a 30-minute wet grinding, 2.5, 5, and 10% LRR used as SCM where the addition of 5% exhibited the highest strength (32.3 MPa) at 28 days compared to the control [9]. However, the study did not explain why the mortar compressive strength did not increase on the 28-days test compared to 7 days. A 120-

minute wet grinding was used for the 0.5-4% LS wet condition addition as a SCM which increases the SAI by 101-128% [14].

Lu et al. [109] used 3-50% industrial slag as a ternary combination with 3-30% LRR as a partial replacement of cementitious material. The study showed that 12% LRR + 18% slag exhibited the highest compressive strengths which were 36 and 60.8 MPa at 7 and 28 days, respectively. Munn et al. [16] used calcined and non-calcined LRR as a partial replacement of cement. The study showed the comparison of 25% LRR with 12.5% LRR + 12.5% FA. The highest 28-days compressive strengths of 25% non-calcined LRR and 12.5% non-calcined LRR + 12.5% FA were 62.3 and 34.4 MPa, respectively. The compressive strength of the ternary mixes reduced significantly while Wu et al. [106] showed that 10% LRR + 10% FA yielded the highest strength in the same comparison. This is probably due to the different origin, physical properties, and chemical composition of LRR. Li et al. [3] compared wet curing with 80^{o}C steam curing mortars containing 20% cement replaced LRR. The compressive strength of the steam cured samples was lower than the wet curing, which was due to the over-steaming of mortar samples at 80^{o}C. The steam cured LRR samples' compressive strength was 35.6% less than the control at 720 days. Qin et al. [34] used Recycled Coarse Aggregate (RCA) concrete by replacing cement with LRR for many combinations. For

10% LRR with 50% RCA, the 28 days compressive strength reached 37.65 MPa, and the SAI for such combination was 115.14%.

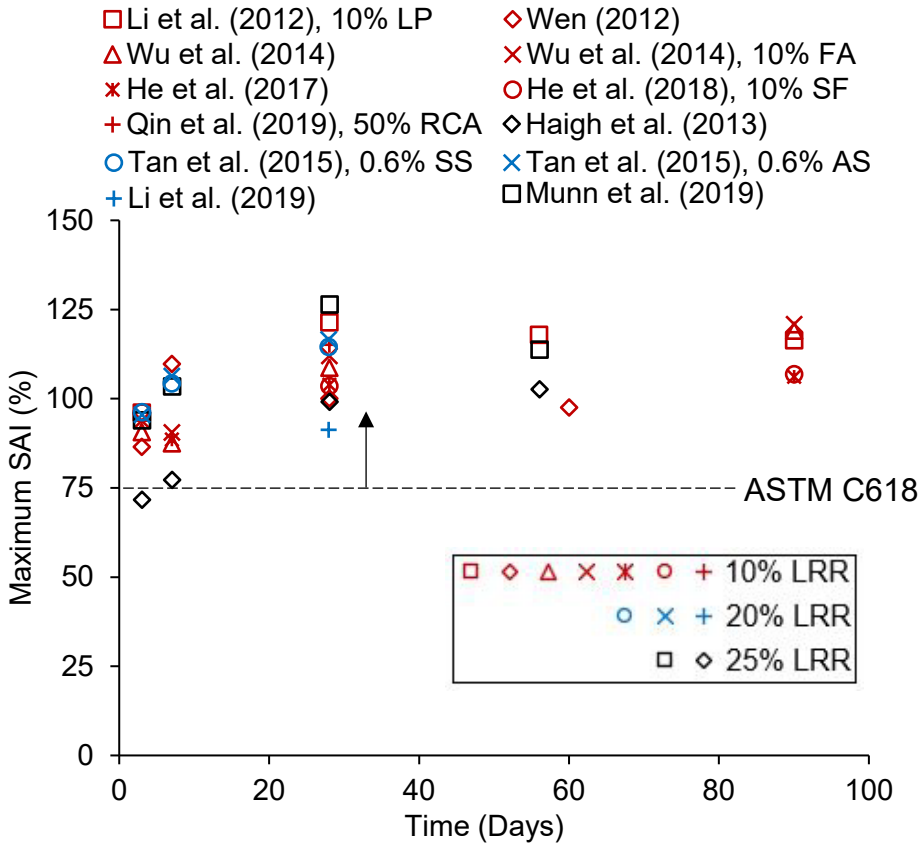

Fig. 9: Maximum SAI by different researchers with respect to various cement replacement percentages (combined and reproduced)

Later, Zhang et al. [20] used 0.03-0.10% TIPA with 30% LRR as a SCM to produce paste samples. The compressive strength of the mix increased with the addition of TIPA. For 0.10% TIPA, the highest compressive strength was 67.4 MPa at 60 days, and the SAI was 118.7%. He et al. [11] used 40 and 60% LRR as SCM to prepare concrete with crushed limestone as coarse aggregate. The study concludes that for 40% and 60% cement replacement, and SCM remains dormant until 180 days after

casting. For 40% LRR, the compressive strength increased by 3.66% after 60 months. Tan et al. [14] used 120-minute wet grinding to prepare micro-LRR mortars, and with 0.5-4.0% cement replacement, the SAI increased from 1.0 to 21.9% at 28 days compressive strength test.

Li and Huang [12] prepared high strength mortars by a ternary combination with 10% silica fume and 2-11% LRR. The study used a maximum 11% LRR by considering mortar flow value of 170 mm as per Lu et al. [109], while ASTM C618 accepts a minimum flow up to 110 mm [40]. It is shown that the increase in LRR contents increases the compressive strength, and the maximum SAI was 99% (112.2 MPa) for 11% cement replacement. Li et al. [13] made a similar study to prepare white Portland cement mortar with 2.5-10% LRR as a pozzolanic material. The maximum compressive strength was 48 MPa, and the SAI was 171% at 28 days.

The scatter plot of Fig. 9 illustrates the maximum SAI of 3-, 7-, 28- 56-, 60- and 90-days compressive strength for the suggested combination by different researchers concerning various cement replacement. the lower data concentration on 56, 60 and 90 days showed a little drop of SAI which indicates that the rate of gain of strength of LRR-cement composites become slower in later ages (56, 60 and 90 days). This phenomenon is very common for cement concrete specimens. Early strength gaining depends on the C3A and C4AF content. Normally, the reactants C2S and C3S remains active after 28 days of hydration which slowly accelerate the hydration reaction. Neville (2012) showed that the strength development of OPC Type -1 with 0.49 w/c is less than 10% from 28 days to 1 year [110]. The horizontal dash line at

75% SAI indicates the ASTM C618 [40] complaint about pozzolanic material and most of the SAIs of different researchers have passed above the code provision.

4.2 Tensile strength, flexural strength, and elastic modulus

Fig. 10 demonstrates the variation of splitting tensile strength with respect to LRR percentage by different researchers [34, 35, 106]. Shi and Zhang [35] used 15-45% LRR as a SCM to prepare high-performance concrete. The study showed that the reduction of splitting tensile strength increased with the cement replacement by LRR at 7 and 14 days. The maximum tensile strength was 6.00 MPa and 6.5 MPa at 7 and 14 days, respectively, and the values were 3.45% and 4.84% higher than that of the control mix. Later, Fu-fei et al. [106] used binary and ternary (10-20% FA) combination with 10-30% LRR to determine the 28-days splitting tensile strength. LRR content of 10% in the binary combination yielded 5.6 MPa, and this was the highest splitting tensile strength. On the other hand, 10% LRR + 10% FA ternary combination samples were approximately 9% higher than the binary sample with maximum tensile strength. Lastly, Qin et al. [34] utilized 10-100% RCA with 10-25% LRR to obtain the split tensile strength of 25 specimens. The maximum tensile strength was 5.04 MPa for 70% RCA + 15% LRR, and the value was 57.5% higher than the control specimen. Shi and Zhang [35] and Fu-fei et al. [106] found the maximum splitting tensile strength for 10% LRR as a partial replacement of cement while, Qin et al. [34] recommended 15% addition of LRR. Though fu-fei et al. [106] used LRR with FA, the result of maximum splitting tensile strength was analogous with Shi and Zhang's findings for binary combination. Apart from these two studies, coarse aggregate replacement by RCA gave a slightly higher use of LRR as a cement replacement.

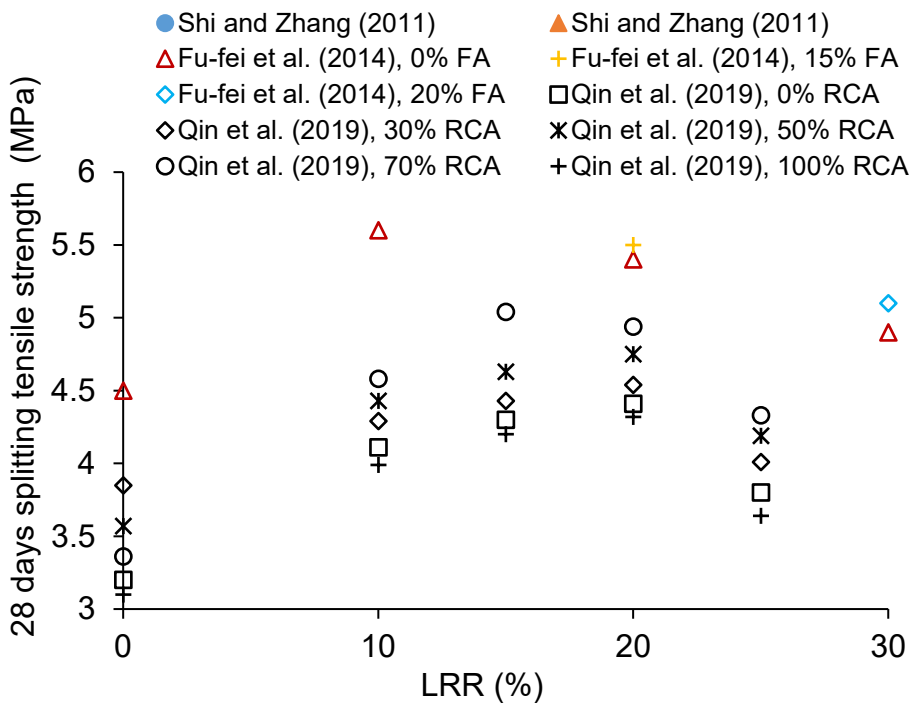

Fig. 10: Variation of splitting tensile strength with respect to LRR content in concrete samples by different researchers (combined and reproduced)

Wen [22] also studied the flexural strength of the green concrete mixed with 10% LRR and 10-40% LP. The author recommended using less than 20% LP. Though 20% LP exhibited the highest flexural strength at 28 days (11 MPa) in their group (10-40% LP), the samples without LP had the maximum value (11.1 MPa). The results suggested using moderate amount of LP with LRR to achieve higher flexural strengths of concrete. Fig. 11 demonstrates the maximum flexural strength of concrete with respect to different percentages of LRR on 28 days.

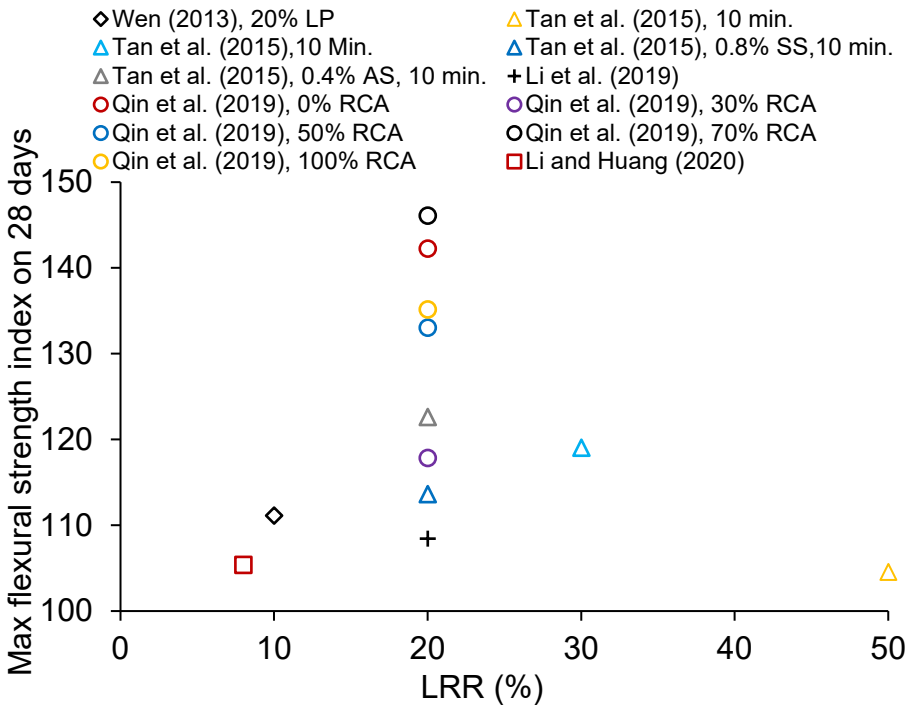

Fig. 11: Graphical representation of maximum flexural strength versus different dosage of LRR content in paste, mortar, and concrete specimens by different researchers (combined and reproduced)

Later, Tan et al. [8] investigated four different combinations in preparing cement paste samples by dry grinding viz. 10-40% LRR + 10 minute grinding (Group I), 50% LRR + 0-20 minute grinding (Group II), 20% LRR + 10 minute grinding + 0.4-0.8% sodium silicate (Group III), and , 20% LRR + 10 minute grinding + 0.4-0.8% aluminum sulfate (Group IV). The median particle size was 14.97, 11.92, 10.85, 9.37, and 8.45 μm for 0, 5, 10, 15, and 20 minutes grinding. The study had shown that the early flexural strength development of 50% LRR cement paste is the slowest while, with aluminum sulfate the process is very rapid. The maximum 28-days flexural strength developed by the groups I, II, III, and IV were 10 (30% LRR), 9.2 (10 minutes), 10 (0.8% sodium silicate), and 10.3 (0.4% aluminum silicate) MPa, respectively.

Li et al. [3] studied flexural strength of 20% LRR and control cement mortar at wet curing and steam curing conditions. As discussed earlier, the study considered high steaming temperature, which diminished early age and long-term strength developments. The flexural strength of 20% LRR at 7 hours steam curing was decreased by 12.2% with respect to wet cured samples on 28 days test. Besides, the flexural strength of the steam cured control specimen was decreased by 7.8% in the same comparison. After that, Qin et al. [34] studied the effect of 0-100% RCA with 0-25% LRR, and the combinations can be divided into five different categories, viz. 0% RCA (Class A), 30% RCA (Class B), 50% RCA (Class C), 70% RCA (Class D), and 100% RCA (Class E). Surprisingly, the maximum flexural strength was yield by 20% LRR in all classes, and the values were 42.3, 17.8, 33, 46.1, and 35.2% higher than the control specimens of their respective classes on the 28-days test. The study concluded that strength development is slower for the higher replacement of LRR in concrete samples. Later, Li and Huang [12] studied the flexural properties of the high strength mortar with a ternary combination of 10% SF and 2-11% LRR. The LRR content of 8% produced flexural strength of 27.2 MPa on 28 days which was the highest among all combinations. The flexural strength increased with the increase of LRR content in the mortar, and the study recommends the content should be less than 8% to have optimum flexural strength.

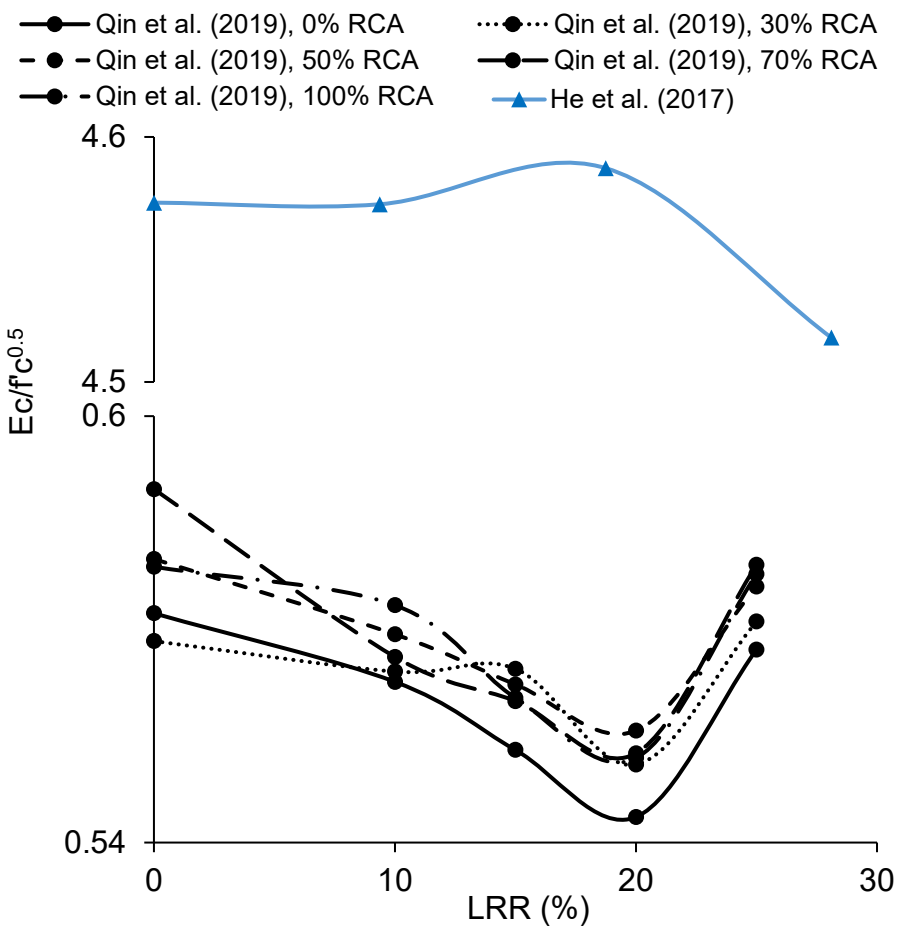

Fig. 12: Combined result of elastic modulus of different researchers with respect to LRR percentage (combined and reproduced)

Fig. 12 shows the variation of elastic modulus (E_C) to square root of 28 days compressive strength (f_c') with respect to the LRR percentage. He et al. [5] reported that the performance of LRR in concrete was decreased at an early age, and the elastic modulus was decreased from 33.23 to 28 GPa for the 30% cement replacement at 7 days test. Surprisingly, the elastic modulus of the LRR specimens increased consistently in 28-, 60- and 90 days tests due to the pozzolanic activity. The maximum elastic modulus was 38.69 GPa for 20% LRR content on 90 days test, and the study recommends using 20% LRR as a pozzolanic material. Later, Qin et al. [34] used 0-

100% RCA with 0-25% LRR as a SCM to generate green concrete. It is clear from the figure that 20% LRR exhibited optimum elastic modulus at 28 days test. In both studies, when the LRR content increased by more than 20% the elastic modulus dropped rapidly regardless of the age.

4.3 Wear loss and impact resistance

Qi et al. [9] used 10-30% LRR as a SCM to study the wear loss of the concrete specimens following JTG E30 [111] highway engineering and cement concrete testing standard at 28 days. The study recommends using less than 20% LRR to have minimum wear loss (3.4 kg/m^2), and the value is approximately 43.33% less than that of the control specimen. Similarly, Li and Huang [12] studied the wear loss with respect to 2-11% cement replacement by LRR to produce high strength mortar specimens (150 x 150 x 150 mm^3) with similar code provision. The study shows that for 11% LRR, the wear loss was 0.82 kg/m^2, which was approximately 44.6% less than the control specimen. Both studies had similar findings with respect to the use of the LRR as a partial replacement of cement. The study assumed that the use of LRR in resisting wear loss is dependent on specimen size and LRR percentage. Li and Huang [12] also investigated the impact resistance of the mortar specimens by dropping 5.2 kg weight with a fall height 1m after 28 days of curing. The study showed that with the increase of LRR content in mortar, the impact resistance increases and more than 5% LRR as a SCM reduced the impact resistance. For 5% LRR as a partial replacement of cement, the 5.2 kg drop-weight frequency was seven from one meter height and the value was 40% higher than the control.

5. Durability properties

5.1 Alkali silica reaction (ASR), chloride migration, and sulfate attack

Munn et al. [16] carried out ASR assessment as per AS1141.60.1 [112]. The standard sample size was 25 mm x 25 mm x 285 mm, and the prepared samples were soaked in 1M NaOH solution at 80^{o}C. The mixes used reactive aggregate, and the cementitious component variables were general-purpose (GP) cement as control specimen, GP cement + FA, GP cement + calcined LRR, and GP cement + non-calcined LRR. Calcined LRR mortar bar expanded 0.05 and 0.14% on 10-and 21-days test while non-calcined expanded 0.10% and 0.39% in the same comparison. Besides, calcined LRR extended 3.96% and 11.76% more than the FA specimens on the test days specified above. The study on ASR by using LRR also showed compliance with ASTM C1567 [113].

Qi et al. [9] replaced 10-30% cement with LRR to examine the concrete chloride penetration for 6 hours as per GB/T 50082 [114]. The study showed that with the increase of LRR content, the electric flux of the concrete reduced. The minimum value was 1333 coulomb for 30% LRR content which is approximately 43% lower than the control specimen. Later, Li and Huang [12] used 2-11% LRR as a pozzolanic material to prepare high strength mortar by using white Portland cement with similar code provision. The research recommended 8% LRR as the optimum pozzolanic material regarding chloride migration result on a 6-hour test. For the addition of 8% LRR, the chloride migration reduced approximately 22% than the control specimen. Fu-fei et al. [19] explained the effect of the water-cement ratio on chloride ion diffusion coefficient (CIDC) at 28 and 84 days. The research concluded that the increase of CIDC was in

proportion to the water-cement ratio. The findings of this research were similar with the studies of Qi et al. [9] and Li and Huang [12] in terms that the addition of LRR reduced chloride penetration at a higher water-cement ratio. The minimum CDIC was 1.77 x 10^{12} m^2/sec on 28 days for a 0.27 water-cement ratio, and the value was 33% smaller than the control specimen (water-cement ratio 0.27). In addition, the CDIC slightly reduced on the 84^{th} day due to the formation of primary and secondary hydration products. The study also explained that the ITZ of the samples became dense in the latter days, which reduced the chloride ion penetration.

Li et al. [3] studied wet cured and steam cured 20% LRR mortar samples by partial immersion in 99% pure sodium sulfate solution for 720 days. The study used 40 mm x 40 mm x 160 mm sample size, and the maximum mass change was 4%, found for steam cured LRR samples. The mass change was 2.67 times higher than the control sample. The adverse effect of steam curing at 80^{o}C for 7 hours decreased the formation of AFt and AFm, since overheating induced sulfate attack to give higher mass change. The upper and lower parts of the partially immersed samples analyzed in XRD, and thenardite (efflorescence) traces were found in both regions.

5.2 Shrinkage and creep

Several researchers worked on the shrinkage and creep of lithium slag concrete. Haigh et al. [15] had 25 and 40 MPa grades concrete to use 25% LRR as a pozzolanic material. The study showed that 25 MPa LRR concrete had 26.5% higher shrinkage than the FA concrete and 2.3% lower than the control at 56 days. In addition, the 40 MPa LRR concrete had the same shrinkage value as FA concrete and 12% lower than the control specimen in the same comparison. He et al. [23] showed that the increase

of LRR in concrete reduces the shrinkage but, a percentage beyond 30% increases the shrinkage in all ages. For 30% LRR as a SCM, the 28- and 90-days shrinkage were approximately 30 and 27% less than the control specimen, respectively. Also, He et al. [5] and Qi et al. [9] used 10-30% replacement of cement by LRR, and the studies recommended using 20% and 30% LRR, respectively. He et al. [5] showed that 20% LRR reduced the shrinkage by 42 and 27% approximately at 28 and 180 days tests, respectively. On the contrary, Qi et al. [9] indicated that LRR decreased shrinkage strain and an addition of 30% LRR slumped the shrinkage by 37 and 24% at 28 and 180 days, respectively. Though He et al. [5] and Qi et al. [9] had similar mixes, the recommendation of optimum LRR percentages differed. This may be because of the variation in coarse aggregate types, LRR specific surface areas and mix ratios. Munn et al. [16] studied the binary and ternary mixes of calcined and non-calcined LRR with FA. The investigation reported that the calcined ternary mixes performed better in controlling shrinkage strain than the non-calcined specimens, while non-calcined binary mixes performed well than the calcined. Though 12.5% LRR and 12.5% FA is the optimized content, the shrinkage value was 9.3 and 4.3% higher than the 25% FA (control) specimen in the 28- and 56-days tests.

Lastly, Li and Huang [12] replaced 2-11% cement with LRR to prepare high strength mortar samples as per Chinese standard JGJ/T70-2009 [115]. Aforementioned, the study found a similar behavior of LRR in the reduction of shrinkage. The authors explained that as a permeable material, the LRR pore retained free water, which enhanced the water retention of the mortar, and decreased the water vaporization, efficiently lowering its shrinkage. The best composition was at 11% LRR as a SCM. The experimentation reported that 11% LRR slashed shrinkage by a factor of 0.83 and

0.76 in 28- and 56-days test, respectively. Fig. 13 shows the data plot of shrinkage of various studies on 28 days with respect to LRR percentage. The horizontal dash line indicates the AS 3972 complaint where allowable shrinkage was restricted to 600 micro-strain (με) and all the shrinkage data from different researchers are below of the maximum permissible value.

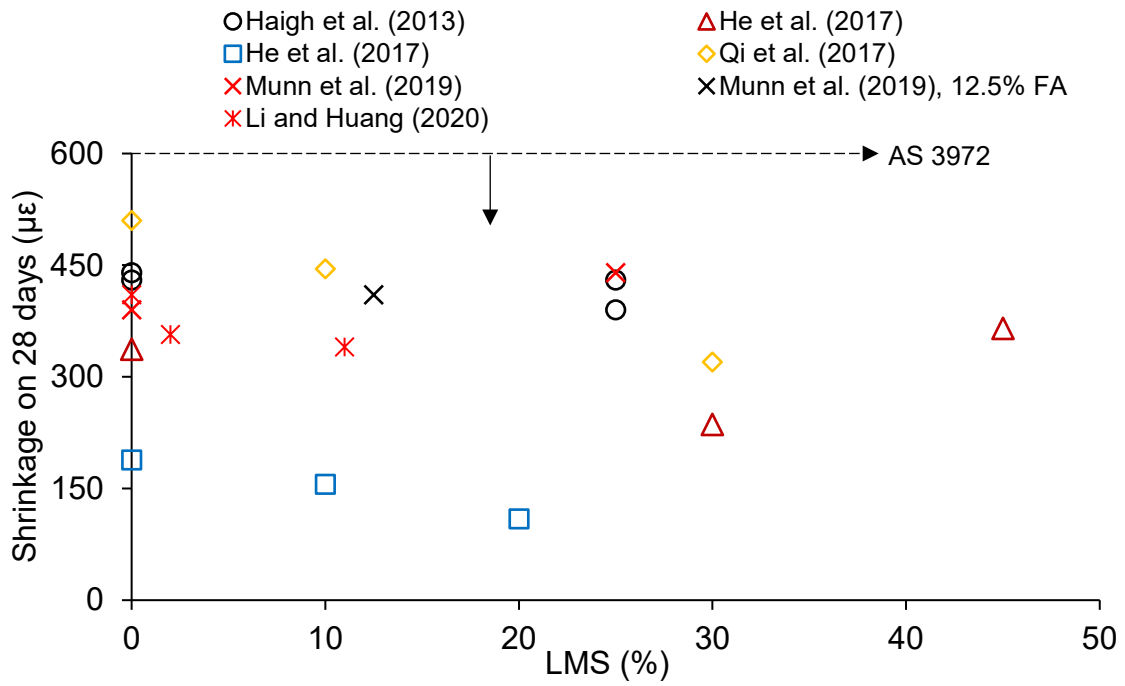

Fig. 13: Data plot of control, maximum and minimum shrinkage with respect to LRR percentage by different researchers (combined and reproduced)

He et al. [5] studied the variation of creep deflection and calculated the creep coefficient of concrete prepared by 10-30% LRR as a SCM. The sample size was 100 x 100 x 300 mm^3, and the dead load was 25% of the 7 days compressive strength. The study also added that 7 days compressive strength was used because, new construction can be started after 7 days instead of 28 days of curing. The minimum creep was found for 20% LRR as a SCM, which was 30% and 29% less than the

control on the 90- and 180-days. The most negligible creep coefficient reported as 1.31 and 1.38 on 90- and 180-days test.

5.3 Sorptivity, carbonation, and water loss

Munn et al. [16] studied the sorptivity of three different types of LRR samples viz. wet, bagged and waxed. The tested sample size was 50 x 50 x 100 mm^3 and kept at 50^oC for 7 days with relative humidity of 50-70%. Non-calcined LRR samples performed better in resisting sorptivity than the FA and calcined samples. The sorptivity values of concrete of 25% wet, bagged, and waxed non-calcined LRR were approximately 18, 17, and 25% less than those of the corresponding concrete samples using calcined LRR. All the samples complied with the ASTM C1585 [113] standard, and the water penetration was well below 25 mm.

Qi et al. [9] determined carbonation depth of 10-30% LRR concrete samples following GB/T 50082 [114] standard. The study showed that increasing LRR content poorly performed in resisting carbonation. The carbonation depth recorded on 3, 7, 14, and 28 days. The minimum and maximum carbonation depth were 5.2 and 10.99 mm at 28 days. The study explained the abrupt increase in carbonation, which was due to reducing the cementitious material into the system. Also, the alkalinity and the neutralization resistance slumped in the progression of CO_2 infiltration onto the surface of the concrete.

Water retention is one of the direct parameters characterizing internal moisture migration of cement-based materials, which has a direct relationship with drying shrinkage of concrete. He et al. [23] studied the water loss of the 15-45% LRR content

concrete samples in reference to Bian et al. [116] and Xinwu [117] studies. The study considered 40 mm x 40 mm x 160 mm sized samples with a water evaporation rate of 2~3.4 g/hour. The study concluded that 30% LRR as a SCM had a minimum water loss, and the value was 46% smaller than the control specimen on 360 days. It is also seen that with the increase of LRR content up to 30%, the water loss reduced periodically but, at 45% LRR content as a pozzolanic material, the value abruptly increased to 170 grams, while for control specimen the water loss was 150 grams. This was due to the excessive volume of the LRR content that could not hydrate due to lack of binding material and absorbed water in the unhydrated region. Tan et al. [14] represented weight loss of the 4% micro-LRR cement paste on 16, 24 hours, and 28 days. The sample size was 40 x 40 x 40 mm^3, and the specified temperature was 50-200^oC. The weight loss of the 4% micro-LRR increased by 39, 19, and 26% on the above specified days with respect to the control specimens. The test on non-evaporable water has a dominant significance over hydration characteristics of LRR. Thus, He et al. [11] determined the non-evaporable water of 40 and 60% LRR content concrete samples at 7, 28, 90 and 180 days. The sample size was 40 x 40 x 40 mm^3, and after employing 105^oC the samples were ground and passed through 80 μm sieve. Later the samples were heated at 1000^oC, and the difference of the weight from 1000^oC and 105^oC recorded. The highest non-evaporable water was found for 40% LRR content samples at 180 days, and the value was slightly higher (2.4%) than the control sample.

6. Microstructural properties

6.1 XRD

The XRD of the hardened LRR mortar products are qualitatively analyzed and graphically depicted in Fig. 14. Karrech et al. [26] studied the use of LS and explained the differences of 29-30^{o} peak in the XRD test is the measure of the degree of C-S-H formation in hardened samples. Zhang et al. [20] explained that the differences of the peak at 9-9.25^{o}, 10.6-10.8^{o}, and 9.75-10.9^{o} would determine AFt, hemicarbonate (HC), and monosulfoaluminate (MS), respectively. Li et al. [3] rigorously studied the hardened products of the LRR mortar through XRD analysis, as shown in Fig. 14 (a). It is seen that the 28 days cured control specimen formed a lower amount of AFt than the 20% LRR sample but produced a higher amount of C-S-H gel in the same comparison. The C-S-H gels are much stronger than the AFt; thus, the compressive strength of the control specimen was approximately 10% higher than the 20% LRR sample at 28 days. After 720 days of wet curing, the 20% LRR mortar produced a higher amount of AFt and C-S-H gel than 28 days of curing. The pozzolanic activity of LRR was activated at later days and consumed more portlandite to form AFm and N(C)-A-S-H gels. Besides, lithium alumino-silicon oxide reacted with cement compounds (like C_3S and C_2S) and decreased with respect to time. As a result, the compressive and flexural strengths of the 20% LRR mortar sample were approximately 8% and 29% higher than that of the control specimen at 720 days curing.

Li et al. [3] also investigated the XRD of the upper and lower portions of the mortar specimens in 5% (by weight) sodium sulfate solution at 720 days, as shown in Fig. 14

(b). The specimens were 40 x 40 x 160 mm^3 and partially immersed in 110 mm under 22 ± 2 ^oC and 55 ± 5% RH. It is evident from the figure that the upper portion of the hardened control specimen produced a higher amount of thenardite than the 20% LRR mortar specimen. The upper portion of the LRR sample also produced a smaller AFt and C-S-H gel than the control. The authors explained that the upper portion was much affected as exposed to physical and sulfate environments than the immersed portion. However, samples containing LRR were less affected by thenardite but produced less hydration products than the control specimen in the sulphate-rich environment. On the other hand, the immersed portion of LRR samples left with unreacted portlandite, albite, and quartz. Though the upper portion of the control samples consumed a higher amount of portlandite than the immersed part, the upper portion had less efflorescence resistive to combined environmental exposures. Likewise, the LRR contained sample had similar behavior in the upper portion of sulfate exposure environment. Overall, from the XRD test result, it is evident that the LRR sample performed better than the control sample. The XRD result also matches the mass change in the mortars under a partially immersed sulfate solution. The LRR mortar had the minimum change in mass and length than the control specimen. Therefore, LRR concrete products are less susceptible to sulfate environments than conventional concrete.

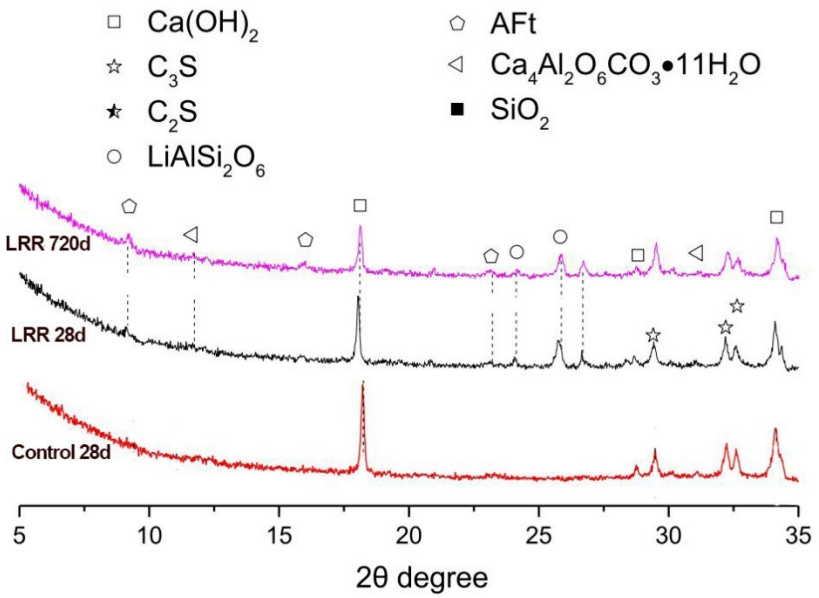
Ca(OH)2
C3S
C2S
LiAlSi2O6
AFt
Ca4Al2O6CO3•11H2O
SiO2
LRR 720d
LRR 28d
Control 28d
5
10
15
20
25
30
35
2θ degree

(a)

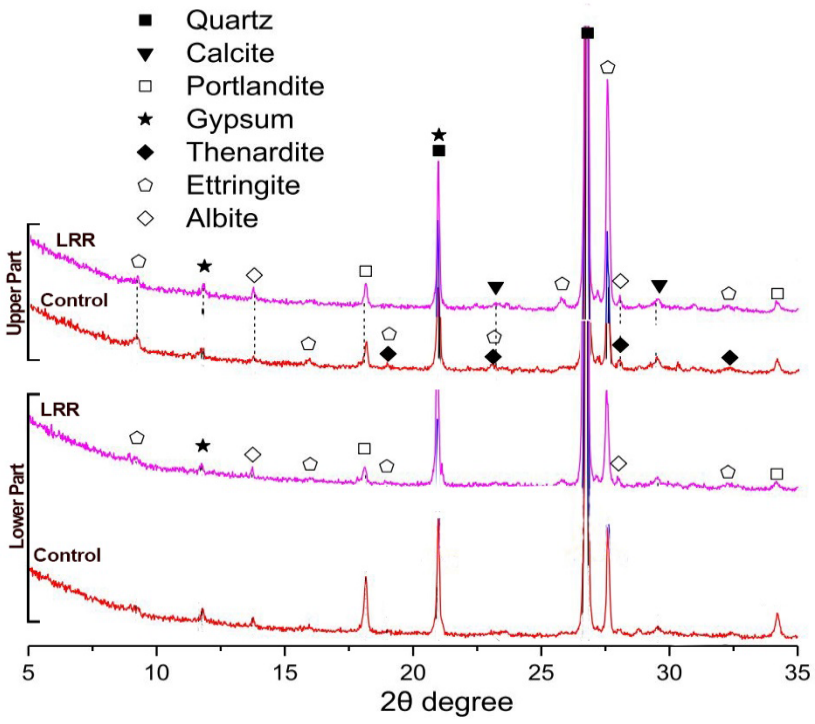
Quartz
Calcite
Portlandite
Gypsum
Thenardite
Ettringite
Albite
Upper Part
LRR
Control
Lower Part
LRR
Control
5
10
15
20
25
30
35
2θ degree

(b)

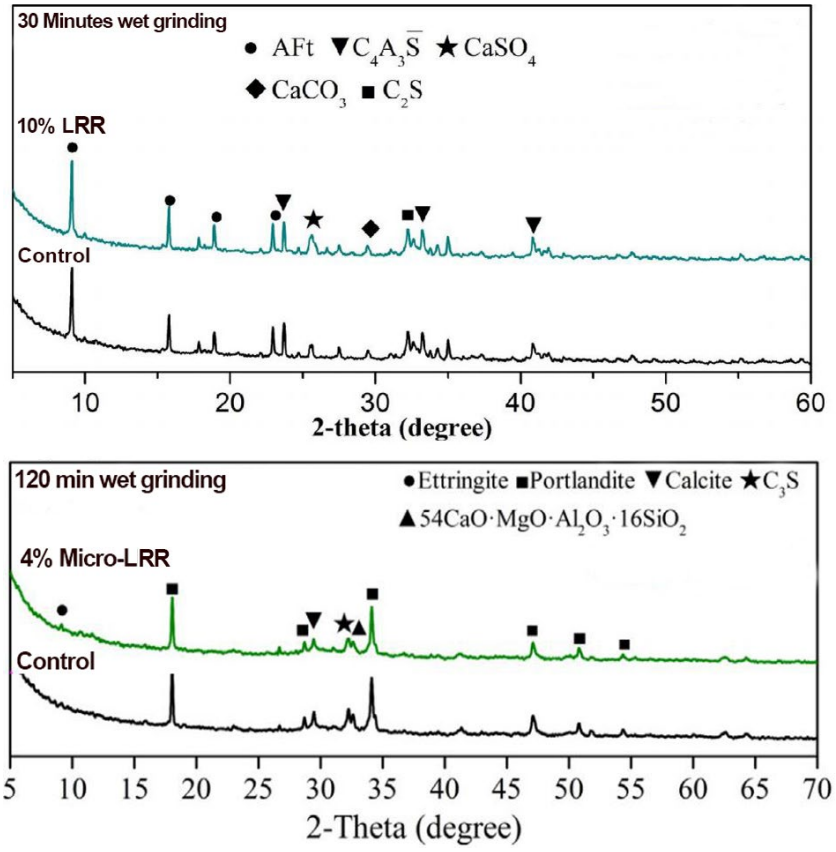

(c)

Fig. 14: XRD of (a) 20% LRR mortar samples at 28- and 720-days and control mortar samples at 28 days normal curing [3], (b) upper and immersed portion of the samples in 5% (by weight) sodium sulfate solution at 720 days [3], and (c) 10% LRR (30 minutes wet grinding) and 4% micro-LRR (120 minutes wet grinding) at 28 days curing [10, 14] (combined from discreate diagrams)

Tan et al. [10, 14] studied the XRDs of 4% (120 minutes wet grinded) and 10% (30 minutes wet grinded) LRR mortar specimens, and the data are compared with the control specimen at 28 days normal hydration. The hydration products like AFt and C-S-H of the 4% micro-LRR mortar samples were much higher than the control specimen (See Fig. 16c). The LRR contained samples also consumed much portlandite than the control sample. Likewise, 10% wet grinded LRR mortar samples had higher hydration

products than the control specimen. On the contrary, 10% wet grinded LRR and control specimens had different XRD peak in the region 20-25^{o} than the 4% micro-LRR and its control specimen. This is probably due to the size effect of the LRR, as 120 minutes wet grinded LRR was much amorphous and pozzolanic reactive. consequently, micro-LRR hydrated C_4A_3S to form higher amount of AFt and C-A-S-H gels distributed in different XRD regions [118, 119].

6.2 SEM

Detailed comparisons of SEM images of specimens containing LRR from different literatures are depicted in Fig. 15. He et al. [5] compared the microstructural images of 10-30% LRR contained concrete specimens on 7 and 90 days hydration. In this study, the SEM images of 20% LRR specimen on the specified days are shown in Fig. 15 (a) and (b). The seven-day microstructure seemed weak as it was highly porous with discrete unhydrated LRR particles and lower C-S-H products. On the other hand, the 90 days hydrated product showed a compact mass with no visible pores (Fig. 15b). The unhydrated LRR reacted with albite and belite minerals to produce higher fibrous AFt and C-S-H gels. Besides, microcracks were also visible in the interface C-S-H and AFt. This SEM image characterization also supports the compressive strength development of the LRR inside concrete products. The strength development rate of 20% LRR specimen was 1, 0.335 and 0.42 MPa/day from 7~28, 28~56, and 7~90 days of hydration. The control specimen had 0.51, 0.19, and 0.22 MPa/day in the same comparison.

He et al. [4] investigated the microstructure of the UHPC containing 5-20% SF and 0-15% LRR. In this survey, only the SEM images of 20% SF (control) and 10% LRR +

10% SF specimens were compared at 28 days of hydration and are depicted in Fig. 15 (c) and (d), respectively. The control specimen's SEM image showed a compact microstructure but with some voids. Also, the development of AFt in the control specimen is less than the LRR contained specimen. Fig. 15 (d) clearly showed the development of AFt from the cement unhydrated particles. Besides, 10% SF + 10% LRR sample was highly compacted with no visible voids and produced a higher amount of fibrous 1-3.5 μm AFt, which led to the development of early compressive strength at 146 MPa at 28 days curing. In addition, the LRR contained sample had minor micro-cracks, a high volume of C-S-H gel and a lower amount of unhydrated cement/LRR minerals. Compared with the control specimen, the compressive strength of LRR contained specimen was only 5 and 10 MPa higher on 28 and 90 days, respectively.

Zhang et al. [19] compared the microstructural images of the 30% LRR and 30% LRR + 0.06% TIPA (Fig. 15e-f). TIPA as a conditioner easily combines with ferric oxide and aluminum phase of cementitious material and gave higher hydration products like C-S-H and N(C)-A-S-H gels earlier than conventional concrete production [116-118]. TIPA accelerates the setting time, hydration reaction, pozzolanic reaction, and phase dissolution of the SCMs [119]. The compactness of the 30% LRR contained samples was less and contained a large pore size than the TIPA contained one. Though LRR increases the AFt and C-S-H formation, TIPA made the microstructure flawless. The microcracks in the TIPA samples were less due to the accelerated hydration of the SCM and cement. This also supports the compressive strength at 60 days, where TIPA contained sample had a 7.8% higher strength than the control. The hydration

heat generated by the 30% LRR+ 0.06% TIPA sample was 192.2 J/g, while the control specimen yielded 113.95 J/g.

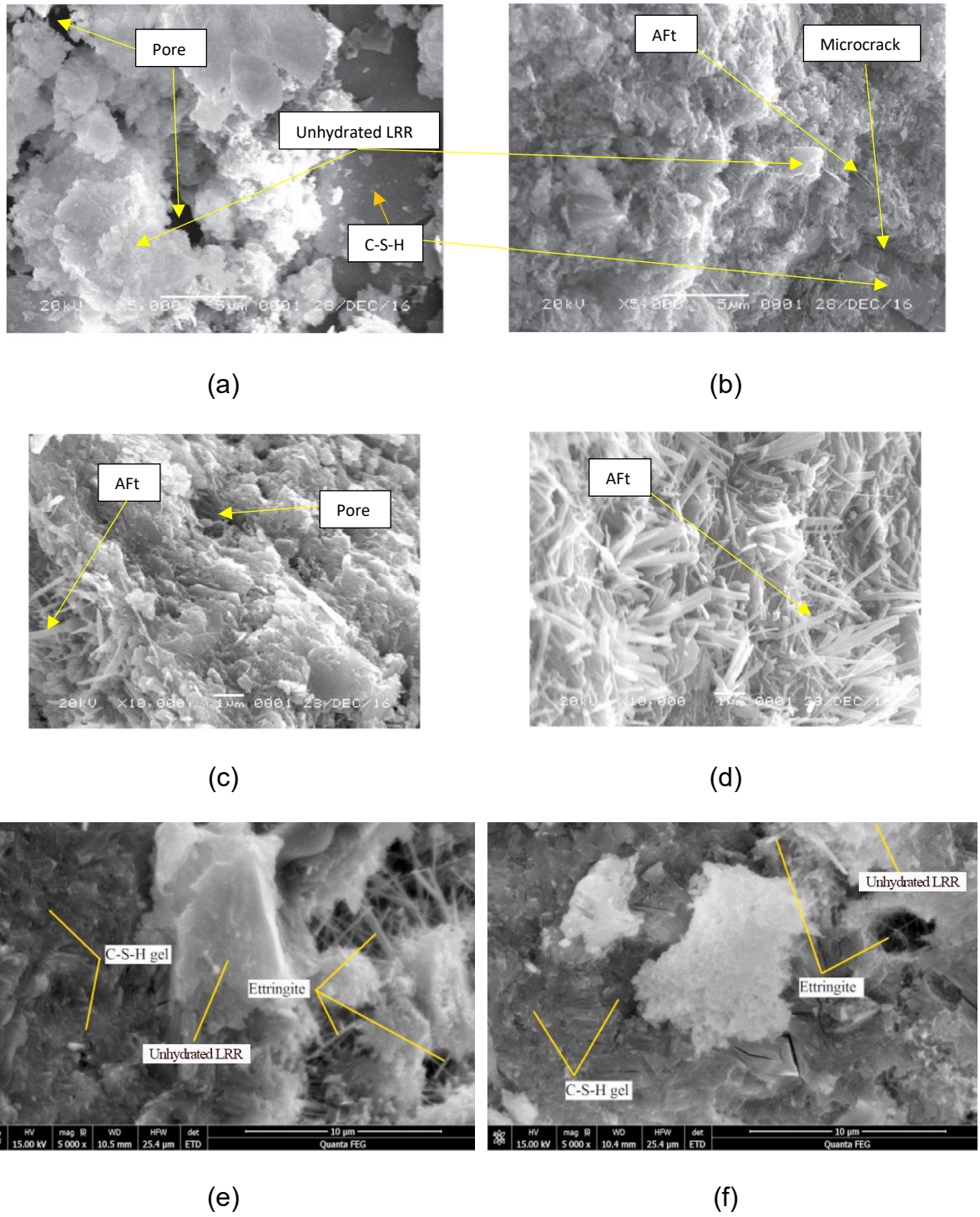

Fig. 15: Comparison of the SEM images: 20% LRR samples on (a) 7 and (b) 90 days hydration [5]; UHPC containing (c) 20% SF (control) and (d) 10% LRR + 10% SF on

28 days curing [4]; mortar containing (e) 30% LRR and (f) 30% LRR + 0.06% TIPA on 60 days curing [20]

6.3 MIP, TGA, nanoindentation, NMR and FT-IR

Fig. 16 shows the variation of the total volume of the void with respect to the LRR amount in concrete specimens. Haigh et al. [15] measured the volume of total voids in control, and 25% LRR contained concrete (designed for 25 and 40 MPa). In both cases, LRR reduced the volume of voids slightly. Later, He et al. [5] compared the pore distribution of the concrete containing 10-30% LRR as SCM on 7 and 90 days. On seven days test, 20% LRR contained sample was 114.4% higher than the control specimen. Surprisingly, the same sample's total pore volume was reduced by 6.75% in the same comparison on 90 days test. Again, He et al. [4] compared the total pore volume of 5-20% SF (control) and 0-15% LRR samples on 3 and 28 days. The test result was similar with He et al. [5] such that, the early age pore volume of the LRR sample was higher than the control and later reduced due to the pozzolanic activity of LRR.

Tan et al. [10] studied the pore size distribution of 2.5% wet grinded LRR containing mortar samples at 1 and 7 days compared with the control specimen. The LRR contained samples slightly reduced the mortar sample's pore volume compared to the control on both test days. Li et al. [3] investigated the total pore volume of control, and 20% LRR contained mortar specimens under both wet curing and steam curing at 28 days. The concrete containing LRR reduced the total void by approximately 8% compared to the control specimen. Surprisingly, over steaming increased the pore volume by 4.24% in the same comparison. Over steaming (at 80^{o}C for 7 hours)

decomposed the AFt and C-S-H, and as a result, the pore volume increased at an early stage and could not recover after further hydration. Next, Tan et al. [14] compared the MIP of control and 4% micro-LRR paste specimens on 1 and 28 days. The study result was anomalous with other preceding studies. 4% micro-LRR increased the total pore volume by 8% in comparison to the control on 28 days test. Conversely, the total pore volume of the LRR contained specimen at 24 hours was 6.31% lower than the control specimen. Lastly, Zhang et al. [20] compared the total voids of 30% LRR (control) and 30% LRR+ 0.06% TIPA samples on 7, 28, and 60 days. LRR and TIPA contained samples that reduced the pore volume consistently with respect to hydration time. 30% LRR + 0.06% TIPA reduced total void by 9.6%, 2.8%, and 1.6% on 7, 28, and 60 days with respect to control specimen.

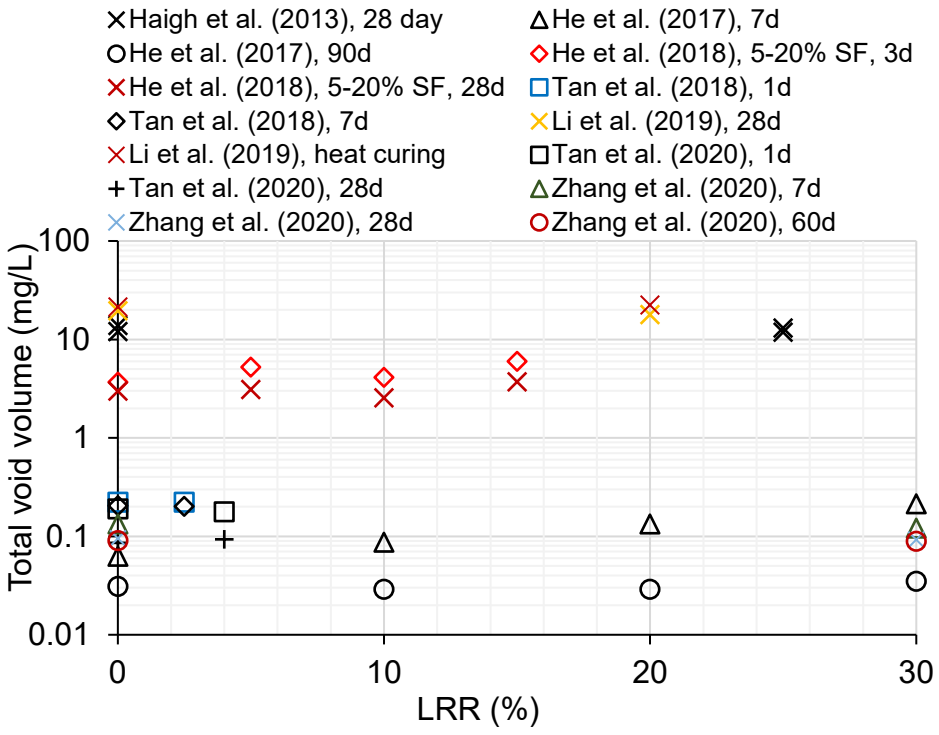

Fig. 16: Semi-logarithmic plot of total volume of void versus LRR percentages in concrete products from different literatures (combined and reproduced)

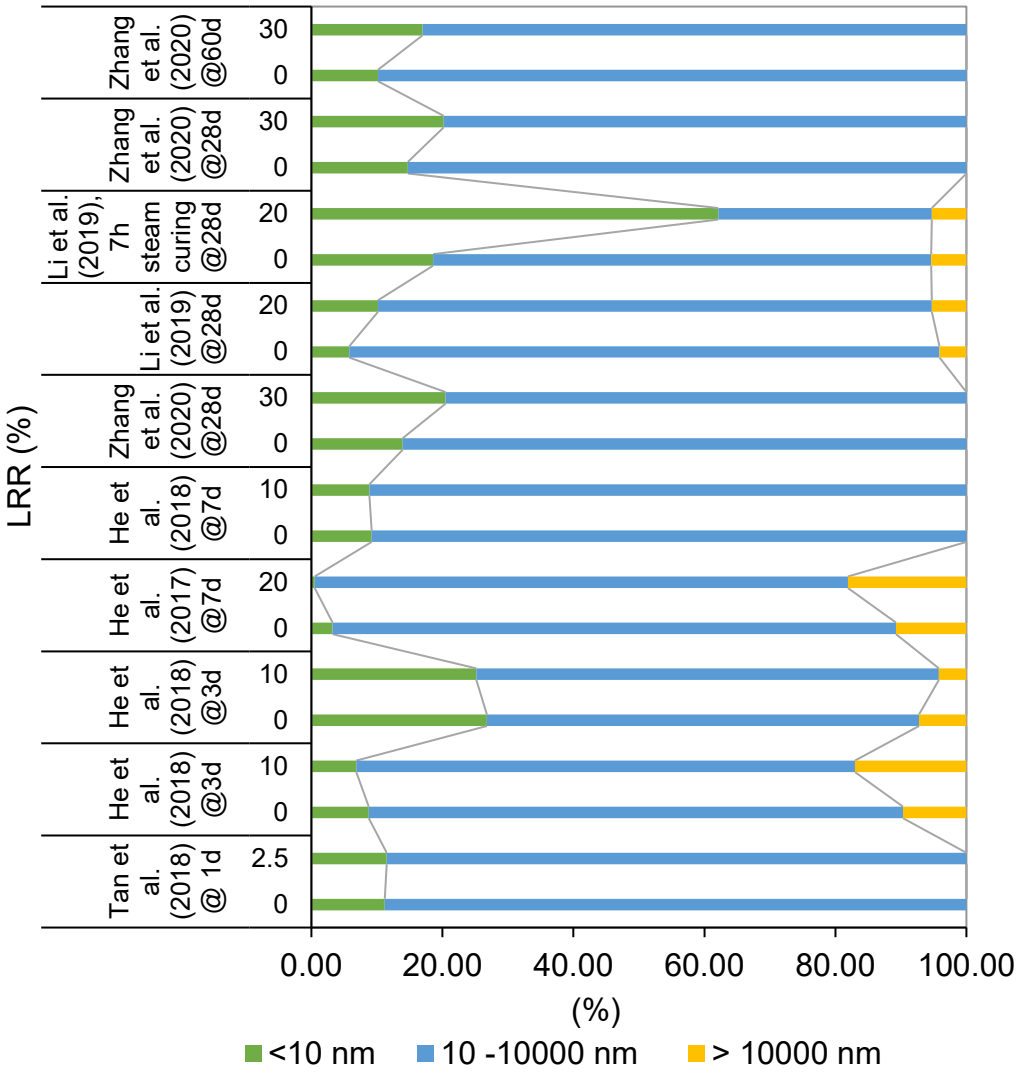

Fig. 17: Distribution of gel pores, capillary pores, and air voids in control and LRR products from different literatures (analyzed, combined, and reproduced)

He et al. [3] categorized the total pore volume into three domains viz. gel pores (<10 nm), capillary pores (10 nm – 10 μm), and air voids (>10 μm). This categorization helps to understand the SCM materials' pozzolanic activity in developing the microstructure state of different products. The MIP curves from different works of literatures were analyzed in the spreadsheet and categorized into three parts as described above and plotted in Fig. 17. He et al. [5] reported that the coupling effect of LRR and pozzolanic activity generates additional AFt and C-S-H, and this help to reduce the large voids in

the long term hydration of the concrete specimens. It is seen from Fig. 17 that LRR is unable to increase the gel pores at an early stage but can increase it by coupled effect. The gel pores are essential, and the bound water inside the gel pores is valuable for further hydration by reducing the capillary and air voids. This further hydration reduces the capillary pores and thereby enhances the mechanical and durability properties. Moreover, changing air voids in LRR products is uncertain and depends on the compaction and mix ratios. Also, steam curing of the LRR products disproportionately increased the gel pores [3]. The air voids keep increasing due to the addition of the LRR in both early and 28 days of age. The mass loss of LRR products from TGA data are analyzed and tabulated in Table 1.

Table 1: Mass loss of LRR products from TGA curve obtained from different literatures at 28 days (analyzed, combined, and reproduced)

Authors	LRR (%)	Mass loss (%)		
		50-200^{o}C	400-500^{o}C	500-1000^{o}C
Li et al. (2019)	20	4.08	1.93	1.51
Li et al. (2019), 7h steam curing	20	1.84	2.65	1.84
Li and Huang (2020)	0	4.47	0.78	-
	11	2.53	0.86	-
Tan et al. (2020)	0	7.4	14.9	2.05
	4	9.2	13.5	2.14
Zhang et al. (2020), 0.06% TIPA	0	8.65	2.3	-
	30	8.99	2.25	-
He et al. (2020)	0	13	4.5	10.3
He et al. (2020), 6% NaOH	24	12.89	2.2	1.6

Li et al. [3] compared the TGA test of normal and heat cured 20% LRR contained mortar. It is seen that 7-hours 80^{o}C steam cured mortar had less mass loss than the normal one. This signifies that the formation of AFt and C-S-H in the steam cured sample was less than that of normally cured. The higher steaming temperature

decomposed AFt and C-S-H products. Besides, the mass loss of steam cured samples at 400-500^{o}C was higher than normal. Though the portlandite consumption was higher, and the higher loss of initial hydration products led to inconsistent strength development. Li and Huang [12] performed TGA tests, and the results were analogous to Li et al. [3]. The 11% LRR contained mortar samples had higher portlandite consumption but lowered initial hydration products. Tan et al. [14] compared the TGA of 4% micro-LRR with the control specimen. The test data showed that LRR samples had lesser initial hydration products and portlandite consumption than the control specimen. Zhang et al. [20] compared the TGA of 30% LRR (control) and 30% LRR + 0.06% TIPA contained mortar specimens. The TGA results of the specimens were similar to Tan et al. [14]. Lastly, He et al. [25] determined the mass loss of the control and 24% LRR + 6% NaOH contained specimens. The initial hydration products and portlandite consumption of the LRR contained sample was less than that of the control. Thus, the 28 days unconfined compressive strength of the LRR contained backfill specimen was 3.3% less in comparison with the control specimen.

He et al. [4, 36] studied the nanoindentation properties of the LRR contained samples, and some significant outcomes are detailed in this study. He et al. [36] detailed the procedure of the nanoindentation test. In a nutshell, the sample is primarily to be intercepted and then cut into small pieces. Later, the small pieces are to be embedded in epoxy resin in a vacuum. This process is followed by grinding and polishing with a confirmation of low surface roughness. Finally, the sample is cleaned in an ultrasonic bath to be examined under the indenter. The nanoindentation test data provides the force-intrusion diagram that explains the porosity, ITZ elastic modulus and hardness. The elastic modulus of the porosity and unreacted cement particles are less than 14

GPa and more than 50 GPa, respectively. The ITZ can be classified into three categories viz. low density (LD), high density (HD), and ultra-high density (UHD) C-S-H, respectively. The LD, HD, and UHD C-S-H elastic modulus are 14-24 GPa, 24-35 GPa, and 35-50 GPa. The LRR contained samples that had higher porosity than the control in both studies. The UHPC formed higher amount of LD, HD, and UHD C-S-H gels than the control specimen, and surprisingly, normal concrete does not form UHD C-S-H. The percentage of the unhydrated particles were 34.8% less than the control specimen [4]. The 20% LRR contained samples reduced LD C-S-H by 18% and increased HD C-S-H by 55.7% compared to the control specimen [36]. The elastic modulus of the ITZ in standard concrete was 19 GPa, and that for LRR contained specimen was 22.3 GPa [36]. In addition, the ITZ elastic modulus of the control UHSC was 36 GPa, and that of the LRR contained sample was 40 GPa [4].

Some studies covered the NMR property of LRR products to understand the formation of Q^0, Q^1, Q^2(0Al) and Q^2(1Al) etc. Tan et al. [14] performed NMR at curing age 16 hours, 24 hours, and 28 days. The study found that Q^1, Q^2(0Al), and Q^2(1Al) increased with increased hydration and Q^0 decreased in the same comparison. At 16 hours elapsed time, Q^2(0Al) and Q^2(1Al) had not formed, and Q^0 shared more than 95% of the formed product. Zhang et al. [20] performed NMR by using 30% LRR +0.06% TIPA and tabulated the formation of Si and Al transformation in making C-S-H and C-A-S-H. The study findings were similar to Tan et al. [14]. TIPA expediated the formation of Q^1, Q^2(0Al), and Q^2(1Al) and significantly reduced the formation of Q^3+Q^4 with the increase of curing days. The aluminum to silicon ratio also continued to increase in the same comparison. Besides, Li et al. [13] measured the FT-IR spectra of 0-5% LRR contained mortar and generated H-O-H vibration at 1422-1462 cm^{-1}, $[SiO]_4$ at 880 to

931 cm^{-1}, and C_3A at 745 cm^{-1}. The peaks of the vibrations in the above-mentioned specified regions increased with the increase of LRR percentage.

7. Conclusion and future work

This paper presents a comprehensive review of particle size, morphology, microstructure and chemical composition of lithium refinery residue, various plastic state properties, harden state mechanical and durability properties of cement concretes containing lithium refinery residue as partial replacement of cement. The following conclusions are derived from the above review:

1. The physical properties of LRR are highly suitable for the use as a pozzolanic material. The composition, particle size, and fineness are essential for the early activation of a product. The catalytic behavior is highly dependent upon the oxide compositions (ASTM C618) and amorphousness. The improved production process can ensure the bulk reuse of LRR in construction products.
2. LRR contains lower lime content, and thus it restricts the higher replacement of the cementitious material in the matrix. The setting times, slump, and exothermic hydration heat generation rate were highly affected but, TIPA, sodium tetraborate, and SAC can enhance the fresh properties. The specific hydration models for the LRR paste have not carried out. Besides, a proper mix design is required to use the LRR in concrete products conveniently.
3. The variation of the mechanical properties of the LRR construction products like paste, mortar, concrete, geopolymer, and backfill was within the standard limits. The previous studies on the use of LRR focused mainly on the

mechanical properties, however, there is a need to study the behaviour of structural members made with concrete using LRR.

4. The work on the durability properties covered a small number of experiments. The studies found the durability parameters are generally within the code limits except the carbonation. However, extensive research is required to establish the durability (like RCPT, ASR, and carbonation etc.) of LRR to be a standard pozzolanic material. In addition, the life cycle assessment of the LRR products is not available in the literatures.
5. The microstructural properties of the LRR products from different literatures are helpful in the explanation of the fresh, mechanical, and durability properties. The microstructural properties like FT-IR and NMR explain the silicon and aluminum bonding and their transformations during hydration. Sufficient experimentation and analytical modeling on the nanoindentation are required to understand the behavior of the hardness of the ITZ of LRR products.

8. Acknowledgements

This research was financially supported by the Australian Research Council (ARC)-DP200102784.

9. Conflict of interests

There was no conflict of interests in this study.

References

1. Karrech, A., et al., *A review on methods for liberating lithium from pegmatities.* Minerals Engineering, 2020. **145**: p. 106085.
2. Jaskula, B.W., *Lithium Production.* USGS Online Publications Directory, 2020. **703**: p. 648-4908.
3. Li, B., et al., *Products and properties of steam cured cement mortar containing lithium slag under partial immersion in sulfate solution.* Construction and Building Materials, 2019. **220**: p. 596-606.
4. He, Z., S. Du, and D. Chen, *Microstructure of ultra high performance concrete containing lithium slag.* Journal of Hazardous Materials, 2018. **353**: p. 35-43.
5. He, Z., L.-y. Li, and S. Du, *Mechanical properties, drying shrinkage and creep of concrete containing lithium slag.* Construction and Building Materials, 2017. **147**: p. 296-304.
6. Rahhal, V. and R. Talero, *Influence of two different fly ashes on the hydration of portland cements.* J. of Thermal Analysis and Calorimetry, 2004. **78**: p. 191-205.
7. Government of Western Australia - Department of Jobs, T., Science and Innovation, *WA Battery Minerals Profile – May* 2020.
8. Tan, H., et al., *Utilization of lithium slag as an admixture in blended cements: Physico-mechanical and hydration characteristics.* Journal of Wuhan University of Technology-Mater. Sci. Ed., 2015. **30**(1): p. 129-133.
9. Qi, L., et al., *Influence of lithium slag from lepidolite on the durability of concrete.* IOP Conference Series: Earth and Environmental Science, 2017. **61**.
10. Tan, H., et al., *Utilization of lithium slag by wet-grinding process to improve the early strength of sulphoaluminate cement paste.* Journal of Cleaner Production, 2018. **205**: p. 536-551.
11. He, Z., et al., *Hydration and microstructure of concrete containing high volume lithium slag.* Materials Express, 2020. **10**(3): p. 430-436.
12. Li, J. and S. Huang, *Recycling of lithium slag as a green admixture for white reactive powder concrete.* Journal of Material Cycles and Waste Management, 2020. **22**(6): p. 1818-1827.
13. Li, J., et al., *Recycling of lithium slag extracted from lithium mica by preparing white Portland cement.* J Environ Manage, 2020. **265**: p. 110551.
14. Tan, H., et al., *Preparation for micro-lithium slag via wet grinding and its application as accelerator in Portland cement.* Journal of Cleaner Production, 2020. **250**.
15. Haigh, M., et al., *Development of New High Performance Supplementary Cementitious Material – A Lithium Production By-Product*, in *CIA Binnual Coference*. 2013, Concrete Institute of Australia (CIA): Australia.
16. Munn, B., I. Dumitru, and D. Maree, *Assessment of the performance of new supplementary cementitious materials from lithium production residues*, in *CIA Binnual Coference*. 2019, Concrete Institute of Australia (CIA): Melbourne, Australia.
17. Zhang, L.F. and R.Y. Wang, *Experimental Study on Alkali-Activated Slag-Lithium Slag-Fly Ash Environmental Concrete.* Advanced Materials Research, 2011. **287-290**: p. 1237-1240.
18. He, Y., et al., *Lithium slag and fly ash-based binder for cemented fine tailings backfill.* J Environ Manage, 2019. **248**: p. 109282.
19. Wu, F.F., K.B. Shi, and S.K. Dong, *Influence of Concrete with Lithium-Slag and Steel Slag by early Curing Conditions.* Key Engineering Materials, 2014. **599**: p. 52-55.
20. Zhang, T., et al., *Effect of TIPA on mechanical properties and hydration properties of cement-lithium slag system.* J Environ Manage, 2020. **276**: p. 111274.
21. Li, H.F., L. Guo, and Y. Xia, *Mechanical Properties of Concretes Containing Super-Fine Mineral Admixtures.* Applied Mechanics and Materials, 2012. **174-177**: p. 1406-1409.
22. Wen, H., *Property Research of Green Concrete Mixed with Lithium Slag and Limestone Flour.* Advanced Materials Research, 2013. **765-767**: p. 3120-3124.
23. He, Z., et al., *Effect of Lithium Slag on Drying Shrinkage of Concrete with Manufactured-sand.* Journal of Residuals Science and Technology, 2017. **14**(1): p. 171-176.

24. Tan, H., et al., *Effect of wet grinded lithium slag on compressive strength and hydration of sulphoaluminate cement system.* Construction and Building Materials, 2021. **267**.
25. He, Y., et al., *Mechanical and environmental characteristics of cemented paste backfill containing lithium slag-blended binder.* Construction and Building Materials, 2021. **271**.
26. Karrech, A., et al., *Sustainable geopolymer using lithium concentrate residues.* Construction and Building Materials, 2019. **228**.
27. Liu, Z., et al., *A green route to sustainable alkali-activated materials by heat and chemical activation of lithium slag.* Journal of Cleaner Production, 2019. **225**: p. 1184-1193.
28. Liu, Z., et al., *Characteristics of Alkali-Activated Lithium Slag at Early Reaction Age.* Journal of Materials in Civil Engineering, 2019. **31**(12).
29. Wang, J., et al., *Setting controlling of lithium slag-based geopolymer by activator and sodium tetraborate as a retarder and its effects on mortar properties.* Cement and Concrete Composites, 2020. **110**.
30. Karrech, A., et al., *Management and valorisation of delithiated β-spodumene and its processing stream.* Case Studies in Construction Materials, 2021. **15**: p. e00671.
31. Karrech, A., et al., *Delithiated β−spodumene as a geopolymer precursor.* Construction and Building Materials, 2021. **309**: p. 124974.
32. Borges, P.H.R., et al., *Lithium Aluminosilicate Residue as Raw Material in the Production of Sustainable Concrete Masonry Units: A Brazilian Case.* The Open Construction and Building Technology Journal, 2016. **10**(1): p. 418-430.
33. Yiren, W., et al., *Micro-morphology and phase composition of lithium slag from lithium carbonate production by sulphuric acid process.* Construction and Building Materials, 2019. **203**: p. 304-313.
34. Qin, Y., et al., *The Mechanical Properties of Recycled Coarse Aggregate Concrete with Lithium Slag.* Advances in Materials Science and Engineering, 2019. **2019**: p. 1-12.
35. Shi, K.B. and S. Zhang, *Ring Method Test on the early-Age Anti-Cracking Capability of High-Performance Lithium Slag Concrete.* Applied Mechanics and Materials 2011. **94-96**: p. 782-785.
36. He, Z., et al., *Nanoindentation Characteristics of Cementitious Materials Containing Lithium Slag.* American Scientific Publishers, 2017. **9 (2)**(6): p. 155-160.
37. Celik, I., *The effects of particle size distribution and surface area upon cement strength development.* Powder Technology, 2009. **188**(3): p. 272-276.
38. Peng, Z., et al., *From ferronickel slag to value-added refractory materials: a microwave sintering strategy.* Resources, Conservation and Recycling, 2019. **149**: p. 521-531.
39. Donatello, S., M. Tyrer, and C.R. Cheeseman, *Comparison of test methods to assess pozzolanic activity.* Cement and Concrete Composites, 2010. **32**(2): p. 121-127.
40. ASTM C618, *Standard Specification for Coal Fly Ash and Raw or Calcined Natural Pozzolan for Use in Concrete*. 2019, American Society for Testing Materials: USA.
41. Prasad, M., K. Reid, and H. Murray, *Kaolin: processing, properties and applications.* Applied clay science, 1991. **6**(2): p. 87-119.
42. Kakali, G., et al., *Thermal treatment of kaolin: the effect of mineralogy on the pozzolanic activity.* Applied clay science, 2001. **20**(1-2): p. 73-80.
43. Heah, C.Y., et al., *Effect of curing profile on kaolin-based geopolymers.* Physics Procedia, 2011. **22**: p. 305-311.
44. Lotfy, A., et al., *Effect of kaolin waste content on the properties of normal-weight concretes.* Construction and Building Materials, 2015. **83**: p. 102-107.
45. Okoye, F.N., J. Durgaprasad, and N.B. Singh, *Fly ash/Kaolin based geopolymer green concretes and their mechanical properties.* Data Brief, 2015. **5**: p. 739-44.
46. Shafiq, N., et al., *Calcined kaolin as cement replacing material and its use in high strength concrete.* Construction and Building Materials, 2015. **81**: p. 313-323.

47. Abbas, R., et al., *Preparation of geopolymer concrete using Egyptian kaolin clay and the study of its environmental effects and economic cost.* Clean Technologies and Environmental Policy, 2020: p. 1-19.
48. Li, S.-Q., et al., *Effect of Kaolin particle size on the removal of Pb (II) from aqueous solutions by Kaolin-supported nanoscale zero-valent iron.* Materials Research Express, 2020. **7**(4): p. 045002.
49. Slatni, I., et al., *Mesoporous silica synthesized from natural local kaolin as an effective adsorbent for removing of Acid Red 337 and its application in the treatment of real industrial textile effluent.* Environmental Science and Pollution Research, 2020. **27**(31): p. 38422-38433.
50. Taklymi, S.M.Q., O. Rezaifar, and M. Gholhaki, *Investigating the properties of bentonite and kaolin modified concrete as a partial substitute to cement.* SN Applied Sciences, 2020. **2**(12): p. 1-14.
51. Wild, S., J.M. Khatib, and A. Jones, *Relative strength, pozzolanic activity and cement hydration in superplasticised metakaolin concrete.* Cement and concrete research, 1996. **26**(10): p. 1537-1544.
52. Ding, J.-T. and Z. Li, *Effects of Metakaolin and Silica Fume on Properties of Concrete.* ACI Materials, 2002. **99-M39**: p. 393-398.
53. Poon, C.-S., et al., *Performance of metakaolin concrete at elevated temperatures.* Cement and Concrete Composites, 2003. **25**(1): p. 83-89.
54. Razak, H.A. and H. Wong, *Strength estimation model for high-strength concrete incorporating metakaolin and silica fume.* Cement and Concrete Research, 2005. **35**(4): p. 688-695.
55. Al-Akhras, N.M., *Durability of metakaolin concrete to sulfate attack.* Cement and concrete research, 2006. **36**(9): p. 1727-1734.
56. Khatib, J., *Metakaolin concrete at a low water to binder ratio.* Construction and Building Materials, 2008. **22**(8): p. 1691-1700.
57. Arikan, M., et al., *Properties of blended cements with thermally activated kaolin.* Construction and Building Materials, 2009. **23**(1): p. 62-70.
58. Badogiannis, E. and S. Tsivilis, *Exploitation of poor Greek kaolins: Durability of metakaolin concrete.* Cement and Concrete Composites, 2009. **31**(2): p. 128-133.
59. Narmatha, M. and T. Felixkala, *Metakaolin–the best material for replacement of cement in concrete.* International journal of advanced research, 2016. **4**(7): p. 1690-1696.
60. Selmani, S., et al., *Effects of metakaolin addition on geopolymer prepared from natural kaolinitic clay.* Applied Clay Science, 2017. **146**: p. 457-467.
61. Fidancevska, E., et al., *Obtaining of dense and highly porous ceramic materials from metallurgical slag.* Science of Sintering, 2003. **35**(2): p. 85-91.
62. Komnitsas, K., D. Zaharaki, and V. Perdikatsis, *Geopolymerisation of low calcium ferronickel slags.* Journal of Materials Science, 2007. **42**(9): p. 3073-3082.
63. Choi, Y.C. and S. Choi, *Alkali–silica reactivity of cementitious materials using ferro-nickel slag fine aggregates produced in different cooling conditions.* Construction and Building Materials, 2015. **99**: p. 279-287.
64. Lemonis, N., et al., *Hydration study of ternary blended cements containing ferronickel slag and natural pozzolan.* Construction and Building Materials, 2015. **81**: p. 130-139.
65. Saha, A.K. and P.K. Sarker, *Sustainable use of ferronickel slag fine aggregate and fly ash in structural concrete: Mechanical properties and leaching study.* Journal of cleaner production, 2017. **162**: p. 438-448.
66. Zhang, Z., et al., *Conversion of local industrial wastes into greener cement through geopolymer technology: A case study of high-magnesium nickel slag.* Journal of Cleaner Production, 2017. **141**: p. 463-471.
67. You, N., et al., *The influence of steel slag and ferronickel slag on the properties of alkali-activated slag mortar.* Construction and Building Materials, 2019. **227**: p. 116614.

68. Liu, Q., et al., *Experimental behaviors of prefabricated members made of ferronickel slag concrete.* Construction and Building Materials, 2020. **261**: p. 120519.
69. Thomas, M. and J. Matthews, *Carbonation of fly ash concrete.* Magazine of Concrete Research, 1992. **44**(160): p. 217-228.
70. Poon, C.S., X. Qiao, and Z. Lin, *Pozzolanic properties of reject fly ash in blended cement pastes.* Cement and Concrete Research, 2003. **33**(11): p. 1857-1865.
71. Li, G., *Properties of high-volume fly ash concrete incorporating nano-SiO2.* Cement and Concrete research, 2004. **34**(6): p. 1043-1049.
72. Siddique, R., *Performance characteristics of high-volume Class F fly ash concrete.* Cement and Concrete Research, 2004. **34**(3): p. 487-493.
73. Atiş, C.D. and O. Karahan, *Properties of steel fiber reinforced fly ash concrete.* Construction and Building Materials, 2009. **23**(1): p. 392-399.
74. Limbachiya, M., M.S. Meddah, and Y. Ouchagour, *Use of recycled concrete aggregate in fly-ash concrete.* Construction and Building Materials, 2012. **27**(1): p. 439-449.
75. Zhao, Q., et al., *Long-age wet curing effect on performance of carbonation resistance of fly ash concrete.* Construction and building materials, 2016. **127**: p. 577-587.
76. Douglas, E., et al., *Alkali activated ground granulated blast-furnace slag concrete: preliminary investigation.* Cement and concrete research, 1991. **21**(1): p. 101-108.
77. Osborne, G., *Durability of Portland blast-furnace slag cement concrete.* Cement and Concrete Composites, 1999. **21**(1): p. 11-21.
78. Li, G. and X. Zhao, *Properties of concrete incorporating fly ash and ground granulated blast-furnace slag.* Cement and Concrete Composites, 2003. **25**(3): p. 293-299.
79. Yüksel, İ., T. Bilir, and Ö. Özkan, *Durability of concrete incorporating non-ground blast furnace slag and bottom ash as fine aggregate.* Building and Environment, 2007. **42**(7): p. 2651-2659.
80. Zhang, L., et al., *Recovery of titanium compounds from molten Ti-bearing blast furnace slag under the dynamic oxidation condition.* Minerals Engineering, 2007. **20**(7): p. 684-693.
81. Bellmann, F. and J. Stark, *Activation of blast furnace slag by a new method.* Cement and Concrete Research, 2009. **39**(8): p. 644-650.
82. Topçu, İ.B. and A.R. Boğa, *Effect of ground granulate blast-furnace slag on corrosion performance of steel embedded in concrete.* Materials & Design, 2010. **31**(7): p. 3358-3365.
83. Huang, H., G. Ye, and D. Damidot, *Effect of blast furnace slag on self-healing of microcracks in cementitious materials.* Cement and concrete research, 2014. **60**: p. 68-82.
84. Aliabdo, A.A., M. Abd Elmoaty, and M.A. Emam, *Factors affecting the mechanical properties of alkali activated ground granulated blast furnace slag concrete.* Construction and Building Materials, 2019. **197**: p. 339-355.
85. Nguyen, H.-A., et al., *Sulfate resistance of low energy SFC no-cement mortar.* Construction and Building Materials, 2016. **102**: p. 239-243.
86. Halder, B., et al. *Influence of coal fly ash on mechanical properties of mortar consisting of total dissolved solids*. in *Proceeding of World of Coal Ash Conference*. 2009.
87. Türker, H.T., et al., *Microstructural alteration of alkali activated slag mortars depend on exposed high temperature level.* Construction and Building Materials, 2016. **104**: p. 169-180.
88. Saha, A.K. and P.K. Sarker, *Potential alkali silica reaction expansion mitigation of ferronickel slag aggregate by fly ash.* Structural Concrete, 2018. **19**(5): p. 1376-1386.
89. Kuri, J.C., M.N.N. Khan, and P.K. Sarker, *Fresh and hardened properties of geopolymer binder using ground high magnesium ferronickel slag with fly ash.* Construction and Building Materials, 2021. **272**.
90. Ramezanianpour, A.A. and M.A. Moeini, *Mechanical and durability properties of alkali activated slag coating mortars containing nanosilica and silica fume.* Construction and Building Materials, 2018. **163**: p. 611-621.

91. Wilson, M.J., L. Wilson, and I. Patey, *The influence of individual clay minerals on formation damage of reservoir sandstones: a critical review with some new insights.* Clay Minerals, 2018. **49**(2): p. 147-164.
92. Abdullah, M.M.A.B., et al., *Clay-Based Materials in Geopolymer Technology*, in *Cement Based Materials*. 2018.
93. ASTM C1872, *Standard Test Method for Thermogravimetric Analysis of Hydraulic Cement*. 2018, American Society for Testing Materials: USA.
94. Liu, P., et al., *Environmental response nanosilica for reducing the pressure of water injection in ultra-low permeability reservoirs.* Journal of Nanoparticle Research, 2017. **19**(12).
95. Douiri, H., et al., *Enhanced dielectric performance of metakaolin–H 3 PO 4 geopolymers.* Materials Letters, 2016. **164**: p. 299-302.
96. Han, J. and P. Yan, *Influence of lithium compound on sulphoaluminate cement hydration process.* Guisuanyan Xuebao(Journal of the Chinese Ceramic Society), 2010. **38**(4): p. 608-614.
97. ASTM C1679, *Standard Practice for Measuring Hydration Kinetics of Hydraulic Cementitious Mixtures Using Isothermal Calorimetry*. 2017, American Society for Testing Materials: USA.
98. BS EN 196-11, *Methods of testing cement. Heat of hydration. Isothermal Conduction Calorimetry method*. 2018, BSI.
99. Deng, H., et al., *Influence of Different Lithium Compounds on Hydration and Mechanical Properties of Calcium Sulfoaluminate Cement.* MDPI, 2020. **13**: p. 16.
100. Cau Dit Coumes, C., et al., *Physico-chemical mechanisms involved in the acceleration of the hydration of calcium sulfoaluminate cement by lithium ions.* Cement and Concrete Research, 2017. **96**: p. 42-51.
101. Deng, Y., C. Zhang, and X. Wei, *Influence of lithium sulfate addition on the properties of Portland cement paste.* Construction and Building Materials, 2014. **50**: p. 457-462.
102. Zhai, M., et al., *Hydration properties and kinetic characteristics of blended cement containing lithium slag powder.* Journal of Building Engineering, 2021. **39**.
103. Dabiĉ, P., R. Krstulovi̇ĉ, and D. Rušiĉ, *A new approach in mathematical modelling of cement hydration development.* Cement and Concrete Research, 2000. **30**(7): p. 1017-1021.
104. Krstulović, R. and P. Dabić, *A conceptual model of the cement hydration process.* Cement and Concrete Research, 2000. **30**(5): p. 693-698.
105. Huang, S.W., et al., *Study on Preparing Aero-Concrete Using Leaching Residual Slag of Lepidolite Ore.* Applied Mechanics and Materials, 2011. **99-100**: p. 375-378.
106. Fu-fei, W., S. Ke-bin, and D. Shuang-kuai, *Properties and Microstructure of HPC with Lithium-slag and Fly ash.* Key Engineering Materials, 2014. **599**.
107. Wei, X. and Z. Li, *Study on hydration of Portland cement with fly ash using electrical measurement.* Materials and structures, 2005. **38**(3): p. 411-417.
108. Tang, S., et al., *The review of early hydration of cement-based materials by electrical methods.* Construction and Building Materials, 2017. **146**: p. 15-29.
109. Lu, J., et al., *Effect of Lithium-Slag in the Performance of Slag Cement Mortar Based on Least-Squares Support Vector Machine Prediction*, in *Materials (Basel)*. 2019.
110. Neville, A.M., *Properties of Concrete*. 5th ed. 2012, UK: Pearson Inc.
111. JTG E30, *Test Methods of Cement and Concrete for Highway Engineering*. 2005, Ministry of Transport: China.
112. AS 1141.60.1, *Methods for sampling and testing aggregates Potential alkali-silica reactivity - Accelerated mortar bar method*. 2014, Standards Australia: Australia. p. 13.
113. ASTM C1567, *Standard Test Method for Determining the Potential Alkali-Silica Reactivity of Combinations of Cementitious Materials and Aggregate (Accelerated Mortar-Bar Method)*. 2021, American Society for Testing Materials: USA. p. 6.
114. GB/T 50082, *Standard for test methods of long-term performance and durability of ordinary concrete*. 2009, China Academy of Building Research: China.

115. 70, J.T., *Standard for test method of basic properties of construction mortar*. 2009, Ministry of Housing and Urban-Rural Development: China.
116. Rongbing, B. and S. Jian, *Synthesis and evaluation of shrinkage-reducing admixture for cementitious materials.* Cement and Concrete Research, 2005. **35**(3): p. 445-448.
117. Shanqing He, X., *Effects of the metakaolin and limestone powderon creep of concrete for bridges.* Journal of China & Foreign Highway, 2014. **34**(6): p. 215–217.
118. Ogawa, K. and D.M. Roy, *C4A3S hydration, ettringite formation, and its expansion mechanism: II. Microstructural observation of expansion.* Cement and Concrete Research, 1982. **12**(1): p. 101-109.
119. Li, M., et al., *Research on the Hydration Properties of C4A3S-CSH2 Cement System at Different Temperatures.* Materials, 2020. **13**(18): p. 4000.